Asghar, M. I. ; Zhang, J.; Wang, H.; Lund, P. D.

Device stability of perovskite solar cells – A review

Published in:
Renewable and Sustainable Energy Reviews

DOI:
10.1016/j.rser.2017.04.003

Published: 01/09/2017

Document Version
Peer reviewed version

Device stability of perovskite solar cells – a review

Authors: M. I. Asghar,[a] J. Zhang,[b] H. Wang[b] and P. D. Lund[a,b]

a) New Energy Technologies Group, Department of Applied Physics, Aalto University, P.O. BOX 15100, FIN-00076 Aalto, Finland.
b) Hubei Collaborative Innovation Centre for Advanced Organic Chemical Materials, Faculty of Physics and Electronic Science, Hubei University, Wuhan 430062, PR China.

Corresponding author: Muhammad Imran Asghar

imran.asghar@aalto.fi

Co-corresponding author: Jun Zhang

gwen_zhang@126.com

Key words: degradation, nano-structure, perovskite, photovoltaic, stability

Abstract:

This work provides a thorough overview of state of the art of stability of perovskite solar cells (PSCs) and covers important degradation issues involved in this technology. Degradation factors, which are reported in the literature affecting the stability of PSCs, are discussed. Several degradation mechanisms resulting from thermal and chemical instabilities, phase transformations, exposure to visible and UV light, moisture and oxygen

and most importantly sealing issues are thoroughly analyzed. Methods are suggested to study most of these degradation mechanisms in a systematic way. In addition, environmental assessment of PSCs is briefly covered. Alternative materials and their preparation methods are screened with respect to stability of the device. Overall, this work contributes in developing better understanding of the degradation mechanisms and help in improving overall stability of the PSCs.

1. Introduction

Dramatic improvement in performance of perovskite solar cells (PSCs) from ~3% to ~22% [1], [2], [3], [4] (certified 21.02% [1]), merely in a short span of less than 10 years, stunned the whole photovoltaic community. It attracted attention of researchers working on various photovoltaic technologies, especially dye solar cell (DSC) and organic photovoltaic (OPV) with emphasis on better efficiency. Interestingly, the researcher's communities belonging to crystalline silicon and thin film solar cell technologies, also showed interest in PSCs for a tandem cell configuration [5], [6].

Although a huge number of articles have been published, demonstrating improvement of PSCs performances, stability of these cells have not been extensively investigated. One of the possible reason for less stability studies, might be lack of understanding of the physical and chemical mechanisms in the device. Generally, high performance PSCs do not retain their efficiencies and degrade in a span of time ranging from few minutes to couple of days, whereas the cells which

demonstrate better stability lacks high performance. To improve the stability of PSCs, systematic understanding of the degradation mechanisms and their effect on the device performance is essential.

The performance of a solar cell is typically expressed in terms of its efficiency (η) obtained through the current-voltage (I-V) parameters including short-circuit current density (J_{SC}), open-circuit voltage (V_{OC}) and fill factor (FF). These performance parameters do not tell much about the degradation mechanisms in the device. In most of the PSCs aging studies, only these performance parameters are reported as a function of time. As a result the cause of the degradation mostly remain unnoticed. A co-relation between the performance parameters of a cell with the chemical and structural changes in nanoscopic scale would make the aging studies more informative and conclusive.

In order to compete with other photovoltaic technologies, PSCs need to pass accelerated aging tests under different stressful conditions. Some of the accelerated ageing tests include: light soaking tests at 60ºC and 85ºC, thermal and humidity cycling tests (85ºC/85RH), UV exposure test etc. Generally, these tests last for 1000 hours. It is noteworthy that stability of PSCs should meet at least stability standards of thin film photovoltaic cells (IEC 61646) in which only 10% decrease in initial performance is allowed over a period of 1000 hours of accelerated aging tests [7], if not of crystalline silicon solar cells (IEC 61215) in which only 5% loss of initial performance is allowed [7], before they can be commercialized. In literature, even lesser stressful tests, e.g. dark test and light soaking test at room temperature, have been reported. In many articles, stability of the cells is not well defined. It is not

clear, how much increase or decrease in performance is allowed before declaring a cell stable. Another question which is not usually addressed is, whether the performance parameters including short-circuit current density (J_{SC}), open-circuit voltage (V_{OC}) and fill factor (FF) need to stable as well, or only efficiency of the cell (η) needs to be stable for a certain time.

This work identifies key challenges related to the stability of the materials used in the PSCs and their effect on the device stability. Furthermore, environmental factors which can influence the stability of the PSC devices, e.g. humidity, temperature and light intensity, are systematically studied with the help of the experimental results reported in the literature. Recommendations are proposed to study the degradation mechanisms with appropriate methods and emphasis is given to find the alternative stable material solutions for PSCs. This study provides a detailed overview of the progress with respect to stability of PSCs.

2. Structure and working principle

The name "perovskite solar cell" originates from the fact that it utilizes perovskite structured light absorbers for photovoltaic activity, like dye solar cells utilize a dye for light harvesting. Perovskite compounds (absorbers in case of PSCs) have a general chemical formula ABX_3, where "A" and "B" are cations of different sizes and "X" is an anion. Equivalent structures of a unit cell of a basic perovskite compound are shown in the Figure 1. Organometallic halide perovskites consisting of an organic cation (i.e. methyl-ammonium $CH_3NH_3^+$, ethyl-ammonium

$CH_3CH_2NH_3^+$, formamidinium $NH_2CH{=}NH_2^+$, cesium Cs), a divalent metal cation of carbon family (i.e. Ge^{2+}, Sn^{2+}, Pb^{2+}) and a monovalent halogen anion (i.e. F^-, Cl^-, Br^-, I^-), are the most relevant ones for PSCs [8],[9].

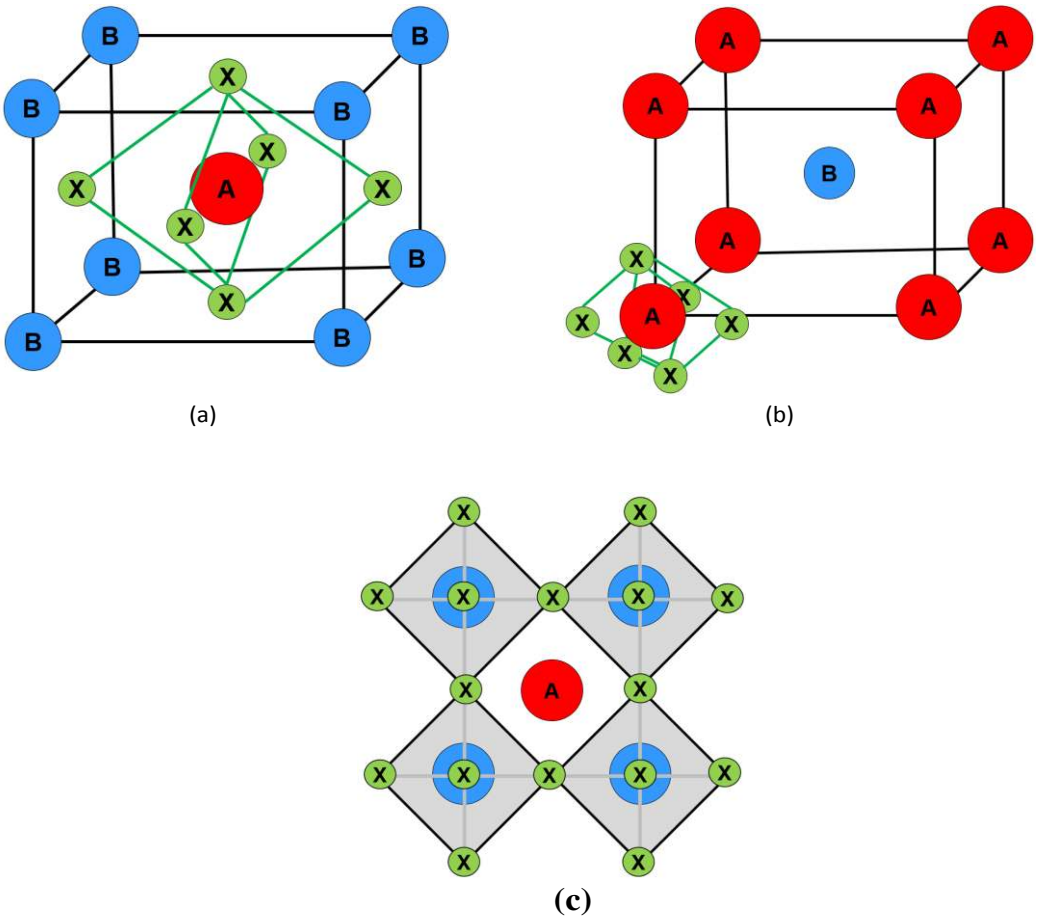

Fig. 1: Unit cell of a basic ABX_3 cubic 3D perovskite structure consisting of A, B and X sites. Please note that the crystal structures shown in (a) and (b) are

equivalent. The structure in (a) is shown so that atom B is at the <0,0,0> position, whereas in structure (b) the atom A is at the <0,0,0> position. In (c), the B-X bonds are represented as an octahedral shape (BX_6). A tilt in this octahedral structure can affect the physical properties of this perovskite material. The lines shown in structures (a), (b) and (c) are only for showing the crystal orientation, not for showing the bonding patterns.

Methyl-ammonium-lead-iodide ($MAPbI_3$) is the most commonly used light absorber [10], [11], [12], [13], [14], [15], [16], [17], [18] . However, the recent trend is to replace $MAPbI_3$ with formamidinium-lead-iodide ($FAPbI_3$) and other potential absorbers mainly due to stability concerns which are explained later in this article. Several composites of organic cations ($CH_3NH_3^+$ and $NH_2CH{=}NH_2^+$) [19], inorganic cations (Cs^{2+} and Sn^{2+})[20] and halide anions (Br^-, Cl^- and I^-) [11], [21], [22], [23], [24], [25], [26], [27] have been employed to improve the device performance and stability.

The tuning of the perovskite $CH_3NH_3Pb(I_xBr_{1-x})_3$ [$0 \leq x \leq 1$] and $CH_3NH_3Pb(Br_xCl_{1-x})_3$ [$0 \leq x \leq 1$] show bandgap tenability in the green-IR region and blue-green region of the spectrum respectively, for optoelectronic applications [28], [29]. The valence band maximum of ABX_3 perovskite structure is made up by the antibonding hybridization of "B = Pb, Sn" s-state and "X = Br, Cl, I" p-state, whereas the conduction band minimum is formed by π antibonding of "B = Pb, Sn" p-state and "X = Br, Cl, I" p-state [30]. Furthermore, "A = methyl-ammonium, formamidinium"

does not directly contribute to the valence band maximum and conduction band minimum, however, it affects the lattice constants and it was found that bandgap increases with increasing lattice parameter [30]. Therefore, selection of all "A", "B" and "X" are critical to the semiconductor and optoelectronics properties (band gap, absorption cross section, charge carrier motilities etc.) of the perovskite structure which eventually affects the performance and stability of the PSCs.

Some of the typical architectures of PSCs are shown in Figure 2. Although PSCs have been manufactured using various structural configurations, primarily there are four types of structures: regular configuration based on the meso-porous scaffold of TiO_2 nanoparticles, the simple planar and heterojunction structure, the meso-porous superstructure and the inverted planar heterojunction as shown in the Figure 2.

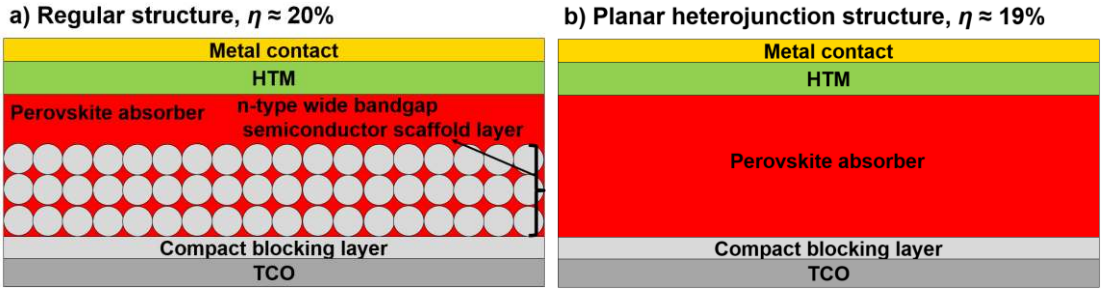

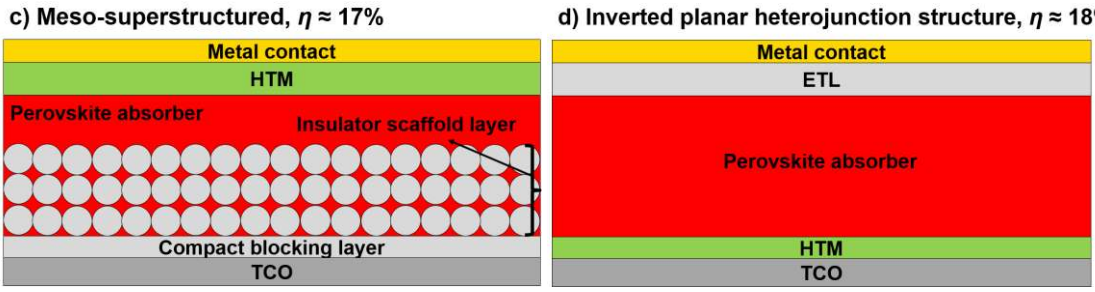

Fig. 2: Different structural configurations of PSCs and their maximum efficiency based on literature, a) regular structure, b) planar heterojunction structure, c) meso-superstructured and d) inverted planar heterojunction structure.

PSCs with regular configuration based on meso-porous scaffold of TiO_2 usually consists of a highly crystalline organic-inorganic halide perovskite absorber, a meso-porous electron transport layer (ETL) and a hole transport material (HTM), sandwiched between a transparent conducting substrate (TCO) and a metal contact. The scaffold film is completely infiltrated or filled with the perovskite absorber and a thin compact layer of TiO_2 on the transparent conducting oxide (TCO) is used to avoid shunting losses.

In planar heterojunction configuration, solid perovskite absorber film is surrounded by non-porous electron and hole selective contacts similar to n-i-p solar cell. In the third configuration which is also known as meso-porous superstructured solar cell (MSSC), meso-porous scaffold layer of inert Al_2O_3 is added. This insulating scaffold layer helps in formation of pin-hole free film and induce n-type properties in scaffold underlying material [31], [32], [22]. In the fourth configuration, the device structure

is inverted by depositing hole selective contact directly onto the TCO substrate and electron selective contact on top of the perovskite absorber. As suggested earlier [31], n-i-p should be referred for regular configuration (Figure 1a,b,c) and p-i-n for inverted configuration (Figure 1d) to avoid any confusion with the conventions used in OPV. Snaith et al. found that although the planar perovskite films have better charge carrier mobility (in excess of 20 $cm^2 V^{-1} s^{-1}$) and emissivity than meso-porous superstructured perovskite films, the presence of sub-gaps states and low intrinsic doping densities limit their photovoltage [32].

Spiro-OMeTAD is the most common HTM material [33], [34], [35], however, other HTMs have been employed as well to achieve over 10% efficiencies (e.g. Triazine-Th-OMeTPA [36], OMeTPA-FA [37], TPA-MeOPh [38], Py-B [39], Py-C [39], P3HT [21] , PTAA [40], TFB [41], M1 [42], carbazole derivatives [43], TBPC [44], conjugated quinolizino acridine based [45], H101 [46], H111 [47], H112 [47], CuSCN [48], [49], CNT based [50] etc). The HTM materials mainly affect the open circuit voltage (V_{oc}) of the cells by decreasing the recombination resistance, though addition of HTM layer would slightly increase the series resistance of the cell.

Gold [51], [52], silver[21], [26], [53], nickel-oxide [54], [55] and carbonaceous materials [56], [57] including carbon nanotubes (CNTs) [58], [50] have been used as contact at cathode. However, XRD measurements in a long term aging experiment at 85ºC showed that Ag was found to be corroded either due to a reaction with perovskite absorber or by gaseous by-products (i.e. HI) from perovskite

decomposition [59]. In addition to typical TCO, that is indium doped tin oxide (ITO) and fluorine doped tin oxide (FTO), aluminium[15], [60], [61], [62], and barium-silver [63] have been used as anode contact in inverse cell configuration. Polymer substrates such as ITO-PET [64], [61], [65] and ITO-PEN [12], [66], [67] have been used resulting in flexible PSCs. In addition, flexible metal substrates for example Ti [68], [69] and stainless steel [70] have also been reported for PSCs.

Due to high sintering temperature i.e. around 450°C for TiO_2 film, the processing of regular PSCs is limited to glass or metal substrates. All other three configurations can be prepared at lower temperature i.e. less than 150°C [71] which enables them to be processed on plastic substrates in addition to glass and metal substrates.

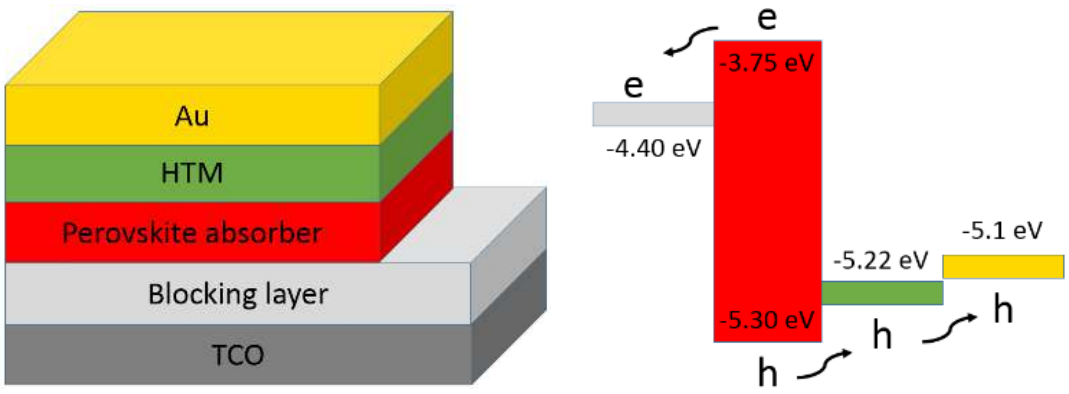

Fig. 3: Schematic structure of a typical PSC and corresponding energy band diagram. The energy levels values are taken from Ke et al. [72]**.**

The working principle of the PSC is still under investigation. Operating mechanisms of DSCs and OPV helps in understanding the functioning of PSCs. A simplified working principle of PSC which is widely accepted is presented as: when the light falls on a PSC, perovskite absorbs light and generates excitons. The electrons and holes pairs are created by the thermal energy, which diffused and get separated through electron and hole selective contacts respectively. Once electrons and holes are present at the anode and cathode respectively, external load can be powered by connecting a circuit through it. Comparable charge carriers diffusion lengths and optical absorption length results in an optimized performance. The operation of planar heterojunction configuration clearly indicates that the photogenerated electrons and holes coexist in the perovskite absorber film and have enough diffusion lengths to reach selective contacts. Xing et al. investigated independently electron and hole diffusion lengths using femtosecond transient optical spectroscopy and found balanced diffusion lengths of at least 100 nm in solution processed $MAPbI_3$ [73]. Stranks et al. have reported diffusion lengths of over 1 µm for both electrons and holes in chloride perovskite i.e. $CH_3NH_3PbI_{(3-x)}Cl_{(x)}$ [11]. Dong et al. reported even larger electron-hole diffusion lengths exceeding 175 µm under 1 Sun (1 W/m^2) and exceeding 3 mm under low light intensity for $CH_3NH_3PbI_3$ single crystals grown by a solution-growth method [13].

Understanding of origins of the electronic and optical properties of the PSCs materials is essential to explain the mechanisms of the devices in detail. Depending on the composition of the materials, their properties significantly affect the

performance of the PSCs. For instance, diffusion lengths of the free charge carriers play a key role in the device performance. It has been observed that conventional perovskite absorber $CH_3NH_3PbI_3$ has lower diffusion length for electrons as compared to that for holes which limits the active layer thickness to only few hundreds of nm. Therefore, usually mesoporous structure is employed when utilizing this absorber. However, composite halide based perovskites, e.g. $CH_3NH_3PbI_{3-x}Cl_x$, improved the electron diffusion length which allow to employ planar structures. Recently, extensive literature has been reported to investigate the absorption, exciton generation and separation, and collection of free carriers in detail [74], [75], [76].

3. Manufacturing methods

Manufacturing method to fabricate a PSC affects both its performance and stability. Spin coating has been widely used for the fabrication of perovskite absorber films[77], [78], [79], [9], [80], [81], [82]. Even the record efficiency of the laboratory scale PSC has been reported using spin coating [4]. The main advantage of this method is to deposit thin films with well defined thicknesses, however, this method is not suitable for upscaling to larger area samples. Another disadvantage of spin coating method is extensive wasting of material which increases the cost of the fabricated device. PSCs have been prepared by various other methods including drop casting[83], spray coating [84], ultrasonic spray coating [85], slot-die coating [86], electrodeposition [87], chemical vapour deposition (CVD) [88], thermal deposition

[89], [90], sequential vacuum deposition [91], doctor blading [92], screen printing [93] and ink-jet printing [94]. Among these methods, drop casting and doctor blading are only suitable for laboratory scale fabrication. Furthermore, it is difficult to control the thickness of a film fabricated through these methods. Especially, in drop casting the differences in particle concentration due to varying evaporation rates may result in variation in the film thickness and composition. Similarly, it is hard to make thin films with slot-die method due to delivery of large amount of solution in the deposition process. Although, spray coating suits for low cost and rapid deposition on large scale, the quality of films is generally not very good due to inadequate film uniformity and steadiness. High quality thin films can be deposited by electrodeposition method, however, this method is costly and time consuming. Chemical vapour deposition is an ideal choice when thin films with good coverage are desired. Furthermore, it is a cost effective method for large scale production. However, high temperatures are needed to improve the quality of the deposited film which may limit the types of substrates used in the PSCs. Thermal deposition is another low-cost fabrication method used for deposition of metals and low melting point materials in vacuum. Unfortunately, the density of the deposited film is generally very low. Sequential vacuum-sublimation method could produce thin crystalline perovskite films with uniformity. Furthermore, this method is suitable for both rigid and flexible substrates due to deposition at low temperature. The Ink-jet printing can deposit very thin films with great precision and excellent controllability. Due to negligible material waste during fabrication, this method is very cost-effective. The major downside of this printing method is that it is rather a

low-throughput process. Screen printing is a low-cost cost and high throughput printing process. Unlike ink-jet printing, screen printing suffers from material waste during deposition. Although most of these methods are low cost and suitable for upscaling of the PSCs, however, promising stability results have been achieved using perovskite absorber films prepared through drop casting method [83], [95] and a solvent engineering process involving spin coating [78], [40].

Nanowire/nanorod of $MAPbI_3$ has been prepared using a small quantity of aprotic solvent in two-step spin coating method, resulting in a power conversion efficiency of 14.71% under AM 1.5G illumination [96]. In another study, Horvath et al. [97] reported fabrication of $MAPbI_3$ nanowires by a simple slip-coating method which is based on low temperature solution mediated crystallization.

In a comparative study [98], it was found that atomic layer deposition (ALD) resulted in a more uniform and less density of pin-holes in hole-blocking compact layers of TiO_2 as compared to the layers obtained by spin coating and spray methods. Another effective method to deposit compact TiO_2 layer, also known as hole blocking layer, by spray pyrolysis [99]. Sol-gel method has been used for electron selective (ZnO) [100] and hole selective (NiO) [101] layers. In another study [102] hydrothermally grown rutile TiO_2 nanorods (~ 0.6 μm) were sensitized with $MAPbI_3$ nanodots and infiltrated with spito-MeOTAD, which resulted in a photocurrent density of 15.6 mA/cm^2 and 9.4% efficiency. Furthermore, Mg doped TiO_2 nanorods by microwave hydrothermal method [103] and Nb doped TiO_2 nanorods grown in a hydrochloric acid solution [104], have been successfully used for PSCs. An efficiency of 11.2%

under simulated AM 1.5 Sun illumination has been reported for PSCs using Yttrium substituted (0.5% Y-TiO_2) TiO_2 with an improvement of 15% in short-circuit current density as compared to pure TiO_2 film [105].

In an effort to replace TiO_2 layer for flexible PSCs applications, ZnO obelisk nanoarrays were synthesized through a mild solution for fabricating PSCs on fibres and textile applications, and demonstrated physical stability by twisting the PSCs fibres and fabrics in three dimensions without obvious damage to the structure [106]. In another nanostructured ZnO scaffold layer study, electrodeposited nanowires of ZnO and their covering by a thin intermediate layer of n-doped ZnO caused an improvement in the charge collection efficiency which resulted in high photocurrent (22 mA/cm^2) and efficiency (10.28%)[107]. Metal contacts (mostly gold or silver) have been deposited mostly by thermal evaporation [16], [88], [90], [108], [109], [110], [111], [112] or sputtering [113], [114], [115], [116].

Tandem cells using perovskite as top cell (due to high open circuit voltage) and crystalline Si or CIGS cell as bottom cell (relatively low open circuit voltage), have been reported. The tenability of optoelectronic properties of perovskite allow optimized performance of the tandem cell which could increase the overall efficiency of the device. Almost 85% of the photovoltaic industry is based on crystalline silicon cells. Their efficiency is between 20-25%. However, with tandem configuration efficiency can be significantly improved at relatively lower cost. Silicon solar cells are generally very stable (over 30 years). Poor stability of PSCs is the limiting factor for application of Si/perovskite tandem cells. Improvement in

PSCs stability would open up possibility of their tandem cells with already established Si or CIGS cells. Since crystalline silicon cells are rigid and opaque, the tandem cells would not be flexible and semi-transparent. However, with perovskite/CIGS configuration a flexible tandem cell with improved performance is possible.

For the mixed-halide hybrid perovskites, the materials are inexpensive to produce; the fabrication methods are relatively simple and can be directly deposited from solution. The lower manufacturing costs and scalable approach are one of the main strengths of alternative technologies such as organic photovoltaics, DSCs and colloidal quantum dot-based solar cells. In terms of cost for PSCs, semiconductor costs, mixed-halide hybrid perovskite cost and other material costs such as conducting glass sheet are low. Although, the cost should also consider the energy output as well as availability of the raw materials, the main hurdle to the further large-scale application of this type of solar cell is the relatively high cost for organic hole conductors. It has been demonstrated that the effective HTM used in PSCs were mainly limited to organic compounds, the state-of-the-art spiro-MeOTAD and other small molecules, such as P3HT, FTAA, PEDOT:PSS. However, compared to other components, the use of HTMs based on organic small moleculars bears a large proportion of cost for PSCs [39]. For example, the most widely used spiro-OMeTAD molecule is relatively expensive due to extensive synthetic processes for preparation. Furthermore, although higher intrinsic hole mobility compared to their amorphous counterpart, polymeric hole-conductors generally still need to be p-doped by

lithium salts in the presence of oxygen in order to achieve comparably high photo-currents [51]. All these limit their approach to low-cost photovoltaic devices.

4. Degradation phenomena in perovskite

4.1. Current status of performance

The current status of performance of PSC technology is that the peak performances for all the four structural configurations range from 17% to 20.1% (regular structure: 20.1% [4], planar heterojunction: 19.3% [33], meso-superstructured: 17% [71] and inverted planar heterojunction: 18% [117]). Table 1 shows the top 10 results in terms of excellent performances for laboratory scale PSCs. Since over 15% efficiencies have been achieved for PSCs using a variety of materials and fabrication processes, it makes the upscaling of PSC technology more appealing than any other emerging low cost photovoltaic technology.

Table 1: State of the art of performances for laboratory scale PSCs.

PSC configuration	η
FTO/bl-TiO_2/mp-TiO_2/$FAPbI_3$/PTAA/Au	20.1% [4]
ITO–PEIE/bl-Ydoped-TiO_2/$MAPbI_{3-x}Cl_x$/spiro-OMeTAD/Au	19.3% [33]
ITO/PEDOT:PSS/$CH_3NH_3PbI_3$/PCBM/Ca-Al	18% [117]
PTAA/$CH_3NH_3PbI_{3-x}Br_x$/mesoporous TiO_2	17.9% [23]
FTO/bl-TiO_2/$MAPbI_3$/spiro-OMeTAD/Ag	17.8% [87]
FTO/bl-TiO_2/mp-TiO_2/$MAPbI_3$/uboid/spiro-OMeTAD/Au	17.1% [118]
FTO/ bl-TiO_2/mp-TiO_2/$MAPbI_3$/spiro-OMeTAD/Au	17.01% [119]
FTO/bl-TiO_2/mp-TiO_2/$MAPbI_3$/pp-spiro-OMeTAD/Au	16.7% [35]
PTAA/$CH_3NH_3PbI_{3-x}Br_x$/mesoporous TiO_2	16.2% [23]
FTO/bl-TiO2/$MAPbI_3$_xClx/spiro-OMeTAD/Ag	15.4% [89]

Similarly, Table 2 shows some results for relatively larger sized PSCs reported in the literature. Generally the efficiencies of the PSCs drop with increase in their active areas due to increase in power losses. However, please note that the literature

data presented in the Table 1 is obtained from PSCs with different structures and configurations. Therefore, the decrease in performance in these relatively large area cells cannot be solely associated with their larger active areas, since other optical and electrochemical factors can also limit the performance of these cells. In a study, a thin (3 µm) flexible PSC with high power to weight ratio (23 Wg^{-1}) was reported with a stabilized efficiency of 12% which was further used to power aviation models successfully [120].

Table 2: State of the art of performances for relatively large size PSCs reported in the literature.

PSC configuration	Active area (cm^2)	η (%)
FTO/NiMgLiO/$MAPbI_3$/PCBM/Ti(Nb)Ox/Ag	1.02	16.2 [78]
FTO/bl-TiO_2/$MAPbI_3$/spiro-OMeTAD/Ag	1.2	15.3 [87]
Oxford PV	1	>10 [31]
FTO/TiO_2/$MAPbI_3$/carbon	4	4.47 [84]
ITO/bl-TiO_2/$MAPbI_3$-xClx/spiro-OMeTAD/Au	4	13.6 [121]

4.2. Current state of the art of stability

Stability is a major concern in the PSCs research field. The cells which gave high performance closer to crystalline-silicon solar cells i.e. around 20%, were degraded rather quickly. In order to compete with other photovoltaic technologies, PSCs must demonstrate long term stability. A sizeable number of stability studies have been performed and reported in the literature. Most of these studies focus on milder accelerated aging tests, for instance, dark tests and light soaking tests at room

temperature or around 60°C using LED light sources or with/without UV filters. Even at these mild conditions, the stable cells have not reached 16% efficiency. For commercialization of PSCs, it is essential that PSCs pass more extreme accelerated ageing tests, for example, damp heat tests at 85°C/85RH and light soaking tests at 85°C with improved performances. The most challenging test would be to pass 1000 hour test without losing 10% performance under AM 1.5 Sun illumination at 85°C/RH. A trend of PSCs performance and stability reported in the literature for the last three years is presented in Figure 4, which clearly shows gradual improvement in stability with increased performance of the PSCs. The improvement in the stability of the devices with improved performance results from the rapid progress in the materials syntheses, especially the light absorber materials; device fabrication procedures and improved understanding of the degradation mechanisms in the device. Chen et al. [78] reported the most efficient PSC which have demonstrated stability (>90% of the initial η) in light soaking test for 1000 h. They utilized highly doped inorganic layers for rapid charge carrier extraction. Furthermore, these layers helped to protect the active materials in the cell from degradation [78]. Table 3 shows some of the important stability results reported in the literature.

Hysteresis has been observed in the current-voltage measurements of PSCs. Some of the speculations about the reason for hysteresis in perovskite-absorber devices are slow dynamic processes originating from the trapping and de-trapping of charge carriers, as well as to changes in absorber or contact conductivity, ferroelectricity,

and ion migration[122], [123], [124], [125]. All of these effects appear to be related to the structural quality of the perovskite layer. The absence of hysteresis in PSCs suggests that perovskite layers are well structured [126].

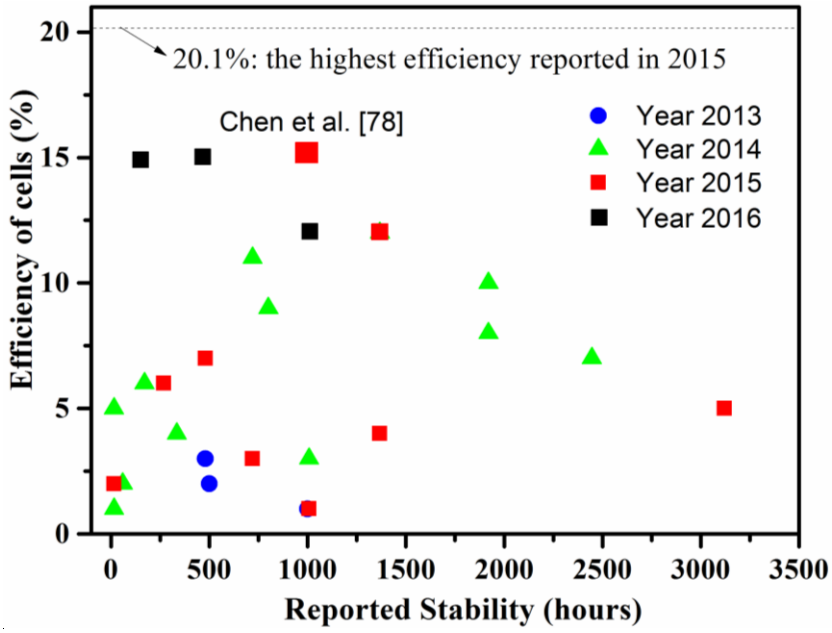

Fig. 4: Trend of performance and stability of PSCs that have been reported in the literature from 2013 to 2016.

Table 3: Accelerated aging tests results for PSCs. Stability results indicate the decrease in performance after the aging test.

Device structure	PSC configuration	Main conclusion/Aims	Degradation avoiding strategies	Initial η (%)	Test condition	Stability result (efficiency loss)

FTO/Ni_xMg_{1-x} LiO/ $MAPbI_3$ / PCBM / $Ti(Nb)O_x$/Ag (sealed)	Inverted planar	Heavily doped inorganic charge extraction layers to achieve very rapid carrier extraction over large areas.	p^+ and n^+ doping by substituting $Ni(Mg)^{2+}$ ions and Ti^{4+} ions on the $Ni_xMg_{1-x}O$ lattice and TiO_x matrix by Li^+ and Nb^{5+} ions, respectively; sealed.	>15	AM 1.5G, 100 mW/cm^2, 1000 h	<10% [78]
FTO/Ni_xMg_{1-x}LiO/ $MAPbI_3$ / PCBM / $Ti(Nb)O_x$/Ag (unsealed)	Inverted planar	Heavily doped inorganic charge extraction layers to achieve very rapid carrier extraction over large areas.	p^+ and n^+ doping by substituting $Ni(Mg)^{2+}$ ions and Ti^{4+} ions on the $Ni_xMg_{1-x}O$ lattice and TiO_x matrix by Li^+ and Nb^{5+} ions, respectively.	>15	Dark at RT 1000 h	3% [78]
TiO_2/ZrO_2/(5-AVA)$_x$(MA)$_{1-x}PbI_3$/C (unsealed)	MSSC	Explore a mixed-cation perovskite (5-AVA)$_x$(MA)$_{1-x}PbI_3$, resulting in a longer exciton lifetime and higher quatum yield for photoinduced charge seperation; HTM free	New perovskite crystal; HTM free	12.8	Ambient air at RT, 1008 h	no loss [83]
TiO_2/ZrO_2/(5-AVA)$_x$(MA)$_{1-x}PbI_3$/C (unsealed)	MSSC	Extensive stability tests to prove the durability of hole-conductor-free PSCs	New perovskite crystal; HTM free PSCs based on a triple-layer architecture employing carbon as a back contact.	~10	80-85°C in dark, 2160 h	7.45% [95]
TiO_2/ZrO_2/(5-AVA)$_x$(MA)$_{1-x}PbI_3$/C (unsealed)				11.4	Outdoor in Jeddah, 168 h	no loss [95]
TiO_2/ZrO_2/(5-AVA)$_x$(MA)$_{1-x}PbI_3$/C (unsealed)				8.2	Light soaking 100 mW/cm^2 (LED) at 45°C in Ar atm. 1056 h	no loss [95]
ITO/PEDOT:PSS/$CH_3NH_3PbI_{3-x}Cl_x$/PC61BM/Ca/Ag (sealed)	Inverted planar	Low-temperature solution processed PSCs; hysteresis-free, highly stable.	$MAPbI_{3-x}Cl_x$ devices instead of $MAPbI_3$ ones; encapsulation.	9.5 (average)	Ambient air at RT, 60 days	<10% [126]
Oxford PV cell (encapsulated)	N/A	N/A	Operated cells with an applied bias; cells are thoroughly encapsulated.	>10	60°C in air, 3000 h	10-15% [31]
FTO/bl-TiO_2/mp-TiO_2/$MAPbI_3$/TSHBC/ graphene/Au (unsealed)	MSSC and planar combined	A functionalized nanographene (TSHBC) is employed as the HTM in PSCs to achieve efficient charge extraction from perovskite.	A new type of HTM.	14.02	240 h, air, RH ≈ 45%, AM 1.5 G, 100 mW/cm^2 illumination	10% [127]
FTO/ZnO NRs/$MAPbI_3$/spiro-OMeTAD/Ag (unsealed)	MSSC	The perovskite $MAPbI_3$ as a sensitizer for ZnO nanorod arrays.	N/A	5.0	500 h, air, RT	13% [128]
ITO/ZnO/MAPbI3/spiro-OMeTAD/Ag (unsealed)	Planar	Low temperature fabrication of ZnO electron collection layer in PSCs; Optimizing the thickness of ZnO layer.	Possible nicely controlled PbI_2 passivation.	13.9	480 h, air	8% [129]
ITO/SnO_2/$MAPbI_3$/spiro-OMeTAD/Ag (unsealed)	Planar	Low-temperature compact SnO_2 thin films as an electron selective contact for PSCs.	The remnant PbI_2 prevents direct contact of SnO_2 and $CH_3NH_3PbI_3$ to reduce the possible degradation.	13	720 h, air	10% [130]
FTO/bl-TiO_2/mp-TiO_2/$MAPbI_3$/TTF-1/Ag	MSSC and planar	An efficient pristine HTM (TTF-1) was introduced for PSCs without using lithium	Avoidance of the use of deliquescent	10	500 h, air, H ~ 40%, RT	<20% [131]

(unsealed)	combined	salts and TBP.	Additives in TTF-1.			
FTO/bl-TiO_2/mp-TiO_2/$MAPbI_3$/HTM/Au (unsealed)	MSSC	Two symmetrical star-shaped HTMs, i.e. FA-MeOPh and TPA-MeOPh with a fused triphenylamine or triphenylamine core and diphenylethenyl side arms were synthesized.	New HTMs were developed; the tight packing of the FA-MeOPh on the $CH_3NH_3PbI_3$ layer.	11.24% for FA-MeOPh; 10.12% for TPA-MeOPh	250 h, air, RT, AM 1.5 G, 100 mW/cm^2 illumination	25.1% for FA-MeOPh; 42.3% for TPA-MeOPh [38]
ITO/NiO_x/$MAPbI_3$/ZnO /Al (unsealed)	Inverted planar	A solution-processed PSC that has p-type NiOx and n-type ZnO nanoparticles as hole and electron transport layers, respectively.	All-metal-oxide charge transport layers.	14.8	1440 h, air, RH: 30-50%, 25 °C	10% [132]
ITO/Cu:NiO_x/$MAPbI_3$/PCBM/Ag (unsealed)	Inverted planar	high-efficiency planar PSCs based on solution processed copper (Cu)-doped NiO_x (Cu:NiO_x) with PCEs up to 15.40% and decent environmental stability.	Employing the Cu:NiO_x as the HTM	15.4	240 h, air	<10% [133]
FTO/bl-TiO_2/mp-TiO_2/$MAPbI_3$/PDPPDBTE/Au (unsealed)	MSSC	Developing new HTM (PDPPDBTE) with high electrical properties and proper oxidation potential with respect to the energy level of of 5.4 eV vs. the vacuum level of perovskite.	The hydrophobic properties of the PDPPDBTE prevented water penetration into the perovskite surface.	9.2	1000 h, air, RH ~ 20%, RT	<10% [134]
FTO/TiO_2/MAPI/P3HT/Au (unsealed)	MSSC	Developing new HTM with high electrical properties and proper oxidation potential with respect to the energy level of of 5.4 eV vs. the vacuum level of perovskite.	The hydrophobic properties of the P3HT prevented water penetration into the perovskite surface.	6.4	1000 h, air, RH ≈ 20%, RT	<10% [134]
FTO/bl-TiO_2/$MAPbI_{3-x}Cl_x$/spiro-OMeTAD/Al_2O_3/Au (sealed)	MSSC	A thin layer of Al_2O_3 nanoparticles employed as a buffer layer sandwiched between the perovskite and the HTM, which inhibits the formation of shunting pathway and allowing for a surgical control of the HTM thickness, and hence leading to a substantial gain in the device FF	Depositing the HTM within an insulating mesoporous "buffer layer" Comprising of Al_2O_3 nanoparticles; sealing cells.	13.07	350 h, AM 1.5 G, 100 mW/cm^2 illumination	<5% [135]
FTO/bl-TiO_2/Al_2O_3/$MAPbI_3$/spiro-OMeTAD/Al_2O_3/Ag (unsealed)	Planar	Molecular structure modeling explains the degradation mechanisms of PSCs and an interface modification method using ultrathin compact Al_2O_3 layers to improve the ambient stability of the PSCs.	The ALD deposited ultrathin Al_2O_3 films coated on the HTM layer to act as a waterproofer and isolated the $CH_3NH_3PbI_3$ layers from moisture.	15.2	576 h, air, RH ≈ 50%, RT	~10% [136]
FTO/bl-TiO_2/mp-TiO_2/$MAPbI_3$/Al_2O_3/spiro-OMeTAD/Au (unsealed)	MSSC	An post-modification of coveraging Al_2O_3 on TiO_2 and perovskite crystals as an insulator barrier to protect $CH_3NH3PbI_3$ from degradation by moisture and suppress electron recombination between TiO_2 and HTM.	Al_2O_3 layer separates $CH_3NH_3PbI_3$ from air and prevents degradation.	4.6	18 h, air, sunlight, RH ≈ 60%, 35 °C	~57% [137]
ITO/ PEDOT:PSS/ VOx / MAPbI3_xBrx/ PC60BM/ Al (unsealed)	Inverted planar	Inherent ionic defects in perovskite layers can degrade the perovskite solar cells (PSCs) even under inert conditions; developing a new concept of a chemical inhibition layer in PSCs using amine-mediated metal oxide systems and realized long-term stable PSCs.	Stable PSCs were achieved by placing an amine-mediated metal oxide (AM-MO) system as a chemical inhibition layer between the $PC_{60}BM$ layer and metal electrode. .	15.02	4000 h, N2 atm., RT 200 h, ambient 9000 h, N_2 atm., RT	~10% [138] 20% [138] 20% [138]

5. Experimental methods to study degradation

In conventional accelerated aging tests, the photovoltaic performance of solar cells in terms of their performance parameters (J_{sc}, V_{oc}, FF, η) is monitored as a function of time. Generally, the standard stability tests last for 1000 hours and the photovoltaic parameters are measured with a certain time period. Although these accelerated aging tests indicate trend of the device performance degradation, however, these tests do not give much information about the reasons leading to such degradation. With such limited information of the cause of degradation, it is difficult to understand the degradation mechanisms, and therefore, it is difficult to overcome such degradation issues. The techniques which give chemical information of the degradation reactions need to be coupled with the conventional photovoltaic measurements in stability testing of solar cells to get a wider view of the degradation phenomena.

For a systematic study of the degradation mechanisms in PSCs, measurement techniques can be divided into two categories: in-situ and ex-situ techniques. In-situ techniques can be applied on the PSCs without damaging the cells. Thus, it is possible to continuously examine the cells during the aging tests using in-situ techniques. On the other hand, ex-situ techniques are destructive in nature. Therefore, ex-situ techniques do not allow continuous monitoring of the cells, but rather provide detailed post-mortem analysis of the degradation mechanisms. The in-situ techniques are primarily based on optical, electrical and electrochemical measurements, and include current-voltage measurement (IV) under 1 Sun lighting

condition [139], electrochemical impedance spectroscopy (EIS) [139], incident-photon-to-collected-electron efficiency (IPCE) technique [140], Raman and FTIR spectroscopy [141], spatially-resolved photocurrent [142], intensity modulated photovoltage spectroscopy (IMVS) [143], intensity modulated photocurrent spectroscopy (IMPS) [143], time-resolved transient measurements [144], imaging techniques [145], image processing method [146], and other optical transmittance and reflectance measurements [139], [147]. The ex-situ techniques generally consist of optical and electron microscopic techniques, and include scanning electron microscope (SEM) [148], focused ion beam (FIB) assisted SEM [149], transmission electron microscope (TEM) [150], energy dispersive X-ray spectroscopy (EDS) [151], electron energy loss spectroscopy (EELS) [152], scanning tunnelling microscopy (STM) [153], atomic force microscopy (AFM) [154], X-ray diffraction (XRD) [155], mass spectroscopy (MS) [156], time of flight-secondary ion mass spectroscopy (TOF-SIMS) [151], [149], nuclear magnetic resonance (NMR) [143], [157], surface photovoltage (SPV) [158], [143], X-ray photoelectron spectroscopy (XPS) [151], [159], photoluminescence (PL) [160], [161], electron beam induced current (EBIC) [74], [162] etc. Some in-situ techniques can be used for studying components of the PSCs such as Raman [163], [164], FTIR [40], [165], image processing method [146], and other optical [147] and electrochemical techniques [146].

Photovoltaic performance parameters (η, J_{sc}, FF, V_{oc}) are extracted from the IV measurements under 1 Sun light intensity. Any degradation in the cell is reflected by the decrease in the values of these performance parameters. However, this does

not necessarily tell the cause of the degradation. In the regard, EIS and IPCE are especially useful to figure out which component of the cell suffers from degradation. Nevertheless, sometimes due to the overlap of the time-constants of different interfaces in the device, it is hard to clearly differentiate the degrading components. Although EIS and IPCE are mostly helpful, these techniques do not tell about the degradation reactions in the device. The techniques which give information of the chemical and structural changes are needed to understand the cause and mechanism of the degradation reaction. Therefore, such techniques (SEM, TEM, AFM, STM, EDS, EELS, Raman, FTIR, PL, XRD etc.) are often used in addition to conventional PV measurement techniques to study the degradation mechanisms. The Table 4 gives an overview of the measurement techniques in a categorized manner. A systematic coupling of the measurements techniques would help to study the degradation of the PSCs (even modules) down to the origin of the cause on atomic level.

Table 4: An overview of measurements methods including the conventional photovoltaic techniques and specific techniques to aid degradation studies in an organized manner.

	Non-destructive / complete PSCs	**Destructive / incomplete PSCs**
Standard PV techniques	**IV:** It tells about the performance parameters of a solar cell (J_{SC}, V_{OC}, FF). Any degradation in these parameters would affect the η of the cells. **EIS:** It gives Impedance losses at different components and their interfaces in the cells. These losses increased as a result of degradation. **IPCE:** It measures the quantum efficiency of a solar cell as a function of wavelength of the incident light.	**Optical transmittance and reflectance:** This measurement gives information of optical changes in individual components of a cell**.** Degradation of a component usually results in higher optical losses. **PL:** It is used to probe discrete energy levels in both intrinsic and extrinsic semiconductors. Degradation

	Degradation of a PSC results in reduced quantum efficiency. **Optical transmittance and reflectance:** This measurement tells us about the optical losses in the cells. These variation in the optical losses can be monitored in-situ during a stability test.	results in shift in the luminescence spectrum affecting the electronic properties of the sample. **EBIC:** It gives information of minority charge carrier's properties and defect density in a semiconductor. Degradation results in reduced minority charge carrier's lifetime.
Techniques giving chemical information	**Raman:** This vibrational spectroscopic measurement technique gives information of the molecular interactions due to the scattering of light in a cell. Characteristic (mostly symmetrical) stretching and bending bands of various chemical bonds (also require change in polarizability) are obtained facilitating to observe any chemical change in the cell. **FTIR:** This vibrational spectroscopic measurement technique gives information of the molecular interactions due to the absorption of IR light in a cell. Characteristic (mostly asymmetrical) stretching and bending bands of various chemical bonds (also require change in dipole) are obtained facilitating to observe any chemical change in the cell. **Image processing method:** It gives information of visual changes in a cell, in terms of its color (R,G,B pixel values) in the space and time coordinates, as a result of degradation.	**SEM:** It gives sample's surface topography to study the morphological changes in the microstructures and their compositions. **TEM:** In this technique, electron beam transmitted through a thin sample gives its microstructural and composition information. **EDS:** It is used for elemental analysis and chemical characterization of a sample. **EELS:** It gives information of atomic composition, chemical bonding, and valence and conduction band electronic properties. **XRD:** It is used for phase identification of a crystalline material. **SPV:** It is used to determine the minority charge carrier diffusion length in a semiconductor. **MS:** It gives information about nature of chemical compounds. It ionizes chemical species and sorts ions based on their mass-charge ratio. **TOF-SIMS:** It is used to determine elemental, chemical state and molecular composition of a solid surface. **Raman:** It gives information of the molecular interactions due to the scattering of light in a cell component. **FTIR:** It gives information of the molecular interactions due to the absorption of IR light in a cell component. **XPS:** It measures the elemental composition and electronic state of the elements present in a material. **AFM:** It is used to study the surface topology and morphology of a sample.

6. Degradation mechanisms: hypothesis and their analysis

There has been several degradation issues reported in the literature for PSCs. In order to systematically study these degradation mechanisms, stability of PSCs can be categorized into intrinsic and extrinsic stability. To study the intrinsic stability of

PSC, it is important to ensure excellent sealing of the device so that external factors such as intrusion of moisture or oxygen, do not influence the device performance. If this objective of preventing external factors affecting the intrinsic stability would be achieved without sealing, it is even better. Intrinsic stability includes the chemical and structural stability of the devices over a range of photovoltaic operating conditions in the presence of the certain amount of impurities, especially oxygen and water, which were already introduced in the device during manufacturing. By photovoltaic operating conditions we mean both the weather conditions (humidity, temperature and light exposure) and the electric bias. The extrinsic stability primarily deals with the failures of sealing and moisture blocking layers. Usually the degradation mechanisms are triggered or accelerated under certain stress conditions. Here, we discuss some of the hypothesis related to important degradation mechanisms.

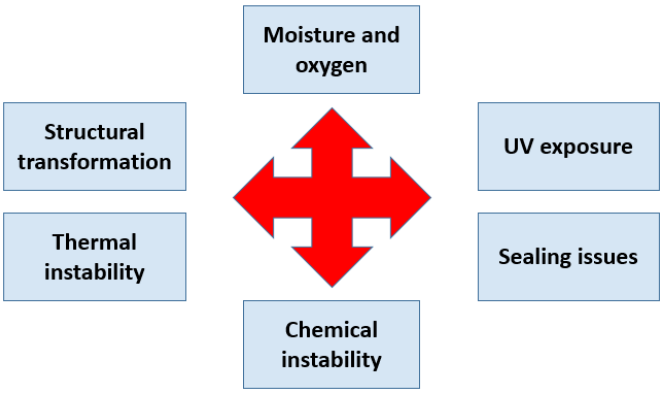

Fig. 5: Degradation issues of perovskite solar cells

6.1 Structural, chemical and thermal instability

The optoelectronic properties (band gap, absorption cross section, charge carrier motilities etc.) of perovskite material depends on its structure. Any crystal distortion due to phase transformation could detrimentally affect its optoelectronic properties which would degrade the photovoltaic performance of PSCs. The stability of a 3D perovskite structure is generally indicated by the Goldschmidt tolerance factor, t:

$$t = \frac{r_A + r_X}{\sqrt{2}(r_B + r_X)}$$

where r_A , r_B and r_X are the radii of monovalent cation, divalent metal cation and monovalent halide anion respectively. Although an ideal 3D cubic perovskite structure has a value of t=1, the perovskite material still keeps 3D cubic structure for $0.9 \leq t \leq 1$. Lowering the value of t lowers the symmetry of the crystal structure. For instance, for $0.7 \leq t \leq 0.9$, the structures are rhombohedral or orthorhombic. A network of BX_6 octahedra is present in the ideal cubic perovskite structure, which may suffer from distortion in lower symmetry structures.

Although there have been many combinations of organic/inorganic cations, metal cations and halide anions used as absorber films in PSCs over the years, $MAPbI_3$ remains the most frequently used absorber film. The major problem with $MAPbI_3$ is that it undergoes an irreversible phase transformation from tetragonal to cubic phase at around 55^{o}C. This phase change is expected to effect the photovoltaic performance of the PSCs. However, some studies show that $MAPbI_3$ still exist as tetragonal phase even after heating to 100 ^{o}C [22], [166], [167], [168], [169]. On the other hand for $MAPbBr_3$ and $MAPbCl_3$, there is

no occurrence of phase transformation for the temperature range relevant to photovoltaic application (i.e. -40°C to 85°C) as shown in the Table 5. Since high solar cell performance has been achieved at 80°C [170], these $MAPbX_3$ perovskites seems to be structurally stable till this temperature. According to one study [171], the temperature of a PSC under the direct sunlight at a temperature of 40°C ambient temperature, would increase to 85°C. The thermal instability of PSC may originate from either intrinsic instability of perovskite film or HTM layer [172]. Coning et al. found that $MAPbI_{3-x}Cl_x$ degraded in inert condition at 85°C due to its intrinsic instability. They further calculated the formation energy of $MAPbI_{3-x}Cl_x$ per unit cell (0.11 eV – 0.14 eV), which was very close to the thermal energy (0.093 eV) calculated at 85°C, therefore degradation of this perovskite film is very likely to occur [173]. In another study, it was found using thermogravimetric analysis (TGA) that the organic component of $MAPbX_3$ (X = I, Cl) was thermally decomposed to HI and CH_3NH_2 resulting in further degradation [174]. Another study showed that thermal conductivity of $MAPbX_3$ is very low in both single crystalline and poly crystalline form, which leads to concentrated heating due to lack of rapid heat spread causing mechanical stresses and degradation of PSCs [175]. In a comparative accelerated aging test, $MAPbBr_3$ was found more thermally stable than $MAPbI_3$ [176]. Furthermore, mixed halide $MAPbI_{3-x}Br_x$ was suggested for thermally stable and efficient PSCs [176].

Table 5: Crystal structure of MAPbX3, where X = I, Br, Cl.

X	Temperature (°C)	Crystal structure
I	T > 54.25	Cubic
	54.25 > T > -110.95	Tetragonal
	T <-110.95	Orthorhombic
Br	T > -36.25	Cubic
	-36.25 > T > -123.65	Tetragonal
	-123.65 > T > -128.65	A slight change in lattice parameters, but still tetragonal
	T < -128.65	Orthorhombic
Cl	T > -94.35	Cubic
	-94.35 > T > -200.25	Tetragonal
	T < -200.25	Orthorhombic

Another organic cation formamidinium (FA) has been used in place of methylammonium (MA). The Goldschmidt tolerance factor for $FAPbI_3$ is larger than $MAPbI_3$ due to its larger cation size. The $FAPbI_3$ undergoes phase transformation to tetragonal crystalline structure at 150°C [177], which indicates larger thermal stability as compared to $MAPbI_3$. It was further supported by a comparative study in which substrates of $MAPbI_3$ and $FAPbI_3$ were heated at 150°C, $FAPbI_3$ substrate showed higher stability (no bleaching for 60 min) as compared to $MAPbI_3$ substrate (bleached in 30 min) [178]. However, $FAPbI_3$ absorber material is very sensitive to moisture and degrades rapidly [178], [168]. It can degrade structurally into a non-perovskite structure composed of 1D chains of edge sharing lead halide octahedral [31]. In another study it was reported that $FAPbI_3$ is known to exist as polymorphs [168]. There are two phases of $FAPbI_3$: a yellow hexagonal phase and a black trigonal phase, which in the presence of solvent can undergo a temperature dependent reversible transition between these two phases [31]. Therefore, stabilization a PSC for long term operation using $FAPbI_3$ is indeed very challenging. Interestingly, $MABr_3$ has been shown to stabilize the $FAPbI_3$ crystal structure [3], [168], [179].

In an effort to replace the organic cations with inorganic cations, Cs cation ($CsPbX_3$) has been reported in PSCs in place of organic cation. $CsPbI_3$ does not form a perovskite crystalline structure at room temperature[180]. $CsSnI_3$ and $CsSnBr_3$ are electrical conductors (p type semiconductor), whereas $CsSnCl_3$ has insulating properties [181]. $CsSnI_3$ undergoes through an irreversible phase transformation from orthorhombic to cubic at 152°C. On the other hand $CsSnBr_3$ remains in cubic structure until it reaches its melting point at 450°C. Unfortunately, the Sn is unstable in its 2^+ oxidation state which can be readily oxidized to 4^+ oxidation state upon exposure to moisture or oxygen, which would result in a self-doping mechanism in the materials causing a significant decrease in the carrier lifetimes in the $ASnX_3$ films [31]. On one side the inorganic perovskite materials have advantage over the organic-inorganic perovskite materials that there is no organic component which could be sensitive to moisture or oxygen, on the other side they are in desperate need of a stable metal cation for a stable PSCs.

Structural and chemical changes degradation of HTM can lead to instability of PSCs. It was proposed that that crystallization of symmetrical spriro-OMeTAD tends to affect the interface between the HTM layer and perovskite film, which can be reduced by introducing local asymmetry into the spiro-OMeTAD [182]. Thermal instability from HTM can be fully avoided by using HTM free PSCs. Using HTM free PSC configuration (For e.g. $TiO_2/ZrO_2/(5\text{-}AVA)_x(MA)_{1-x}PbI_3/C$) PSCs have been reported with excellent thermal stability [95]. One speculation for increased thermal stability is utilization of thermally conductive carbon material which can help in dissipating the internal heat of the PSC.

Therefore, high heat transfer coefficient materials, such as graphene, CNTs, carbon fibers, etc., are very significant for improving the thermal stability of the PSCs [172], [183], [184].

6.2 Oxygen and moisture

Both oxygen and water if present in a PSC above a certain amount, can potentially degrade it over a period of time. Oxygen above a certain limit can result in oxidation of the organic components in the cell. PSCs have been reported to be stored in dry air in the dark without noticeable degradation [166], [167]. It shows that as such oxygen in a dark and dry atmosphere does not harm the stability of the PSCs. However, in the presence of light, the process of photo-oxidation is almost unavoidable in most of the semiconducting materials [185], [186]. In a complete device, the rate of photo-oxidation depends on the relative rates of the oxidation and electron transfer rate. If oxidation rate would be faster than electron transfer rate, there are higher chances of photo-oxidation, whereas, if the oxidation rate is outcompeted by electron transfer rate, there are less chances of photo-oxidation. In a comparative study of photo-oxidation for different PSCs architecture including regular, flat and meso-superstructured using transient absorption spectroscopy, regular structure showed the most promising results due to faster electron transfer rate in the presence of meso-porous TiO_2 film as compared other architectures [187]. In complete planar heterojunction, the electron transfer rate is also very high (5 ns) due to the use of electron accepter either compact TiO_2 or PCBM [11], [73]. The electron lifetimes in PSC employing HTM is in the range of several μs [187], therefore the photo-oxidation is almost negligible.

As proposed by Snaith et al. [31], if there would be proper sealing of PSC, it is resistant to photo-oxidation.

The stability of perovskite absorber films is very sensitive to water. Degradation of PSCs have been reported due to the presence of water in the cells. In addition, polar solvent can also degrade the perovskite materials. Decomposition of perovskite has been reported due to highly hygroscopic nature of the amine salts [188].The most commonly used HTM, spiro-OMeTAD, is also unstable in the presence of water. There have been different mechanisms reported in the literature for water induced degradation in the PSCs. Kamat et al. suggested that presence of water can change the crystalline structure of the absorber film causing dramatic changes in the perovskite ground and excited state absorption spectra [189]. Kelly et al. found that the rate of degradation was related to the humidity level, tens of days for RH level of 50% and less than 3 days for RH level of 80% [190]. Rate of degradation also depends on the layers over the perovskite film, for e.g. relatively hydrophobic materials like P3HT offer better stability as compared to spiro-OMeTAD and PTAA [190].

Barnes et al. illustrated the formation of a monohydrate phase which is in equilibrium with a small amount of the dehydrate phase, depending on the time and intensity of moisture exposure as shown in the following reversible reaction [191], [31].

$$4CH_3NH_3PbI_3 \overset{H_2O}{\Longleftrightarrow} 4[CH_3NH_3PbI_3 \cdot H_2O]$$

$$4[CH_3NH_3PbI_3 \cdot H_2O] \overset{H_2O}{\Longleftrightarrow} (CH_3NH_3)_4PbI_6 \cdot 2H_2O + 3PbI_2$$

Combination of moisture and heat resulted in even faster degradation due to rapid formation of PbI_2 and loss of organic component from the crystalline structure. This degradation process is irreversible unlike the reaction occurred only in presence of moisture. Furthermore, rapid degradation of perovskite structure (<24 h) has been reported also in an electric field in the presence of the water [31]. Degradation reactions because of heat and electric in the presence of water are shown in the following reactions [31].

$$4CH_3NH_3PbI_3 \overset{H_2O}{\Longleftrightarrow} 4[CH_3NH_3PbI_3 \cdot H_2O]$$

$$4[CH_3NH_3PbI_3 \cdot H_2O] \xrightarrow{E-Field} 4CH_3NH_3^+ + 4I^- + 4PbI_2$$

$$4[CH_3NH_3PbI_3 \cdot H_2O] \overset{H_2O}{\Longleftrightarrow} (CH_3NH_3)_4PbI_6 \cdot 2H_2O + 3PbI_2$$

$$4[CH_3NH_3PbI_3 \cdot H_2O] \xrightarrow{Heat} 4CH_3NH_2 + 4HI + 4PbI_2$$

It is suggested that application of electric field causes drift in the loosely bound cations in the hydrated phase, resulting in destabilized PbI_6^{4-} octahedral, which then decompose to PbI_2 and excess iodide [31].

Several approaches have been reported to increase resistance to moisture related degradation in PSCs. First approach is to employ a thin blocking layer (for e.g. Al_2O_3) between the perovskite and HTM [135], [136]. Another approach is to use moisture blocking HTM [131], [170]. Another approach suggest use of hydrophobic carbon electrode [83]. Recently, a triple layer structure consisting of $MAPbI_3$ infiltrated layers of meso-porous TiO_2 and meso-porours ZrO_2, and a thick carbon electrode, has shown excellent stability in humid conditions even at high temperature [95].

6.3 Visible and UV light exposure

Promising stability results have been reported for regular and MSSC under light soaking tests at room temperature as shown in the Figure 6 [16]. However, those tests were performed using LED light source free from UV light. PSCs tend to degrade when light soaked under AM 1.5G 1 Sun light intensity as shown in the Figure 7 [192]. The degradation pattern clearly shows that the drop in efficiency follow the pattern of decreasing J_{sc}. The presence of TiO_2 which is photocatalytic active for the UV light, seems to be the reason for this degradation. Application of UV filter on the PSCs aged under AM 1.5G 1 Sun light intensity, overcomes this degradation [192]. It was observed that the J_{sc} of MSSC remained quite stable when aged under light soaking AM 1.5G at 1 Sun light intensity at open circuit condition as shown in the Figure 8. However, the J_{sc} of MSSC decreased sharply when aged under light soaking AM 1.5G at 1 Sun light intensity at maximum power point (MPPT) condition as shown in the Figure 9 [193]. Again presence of TiO_2 was suspected to be the reason for this degradation at MPPT. It was further confirmed when TiO_2 was replaced with fullerene (C_{60}) in MSSC, the cell became stable even under light soaking at MPPT [193].

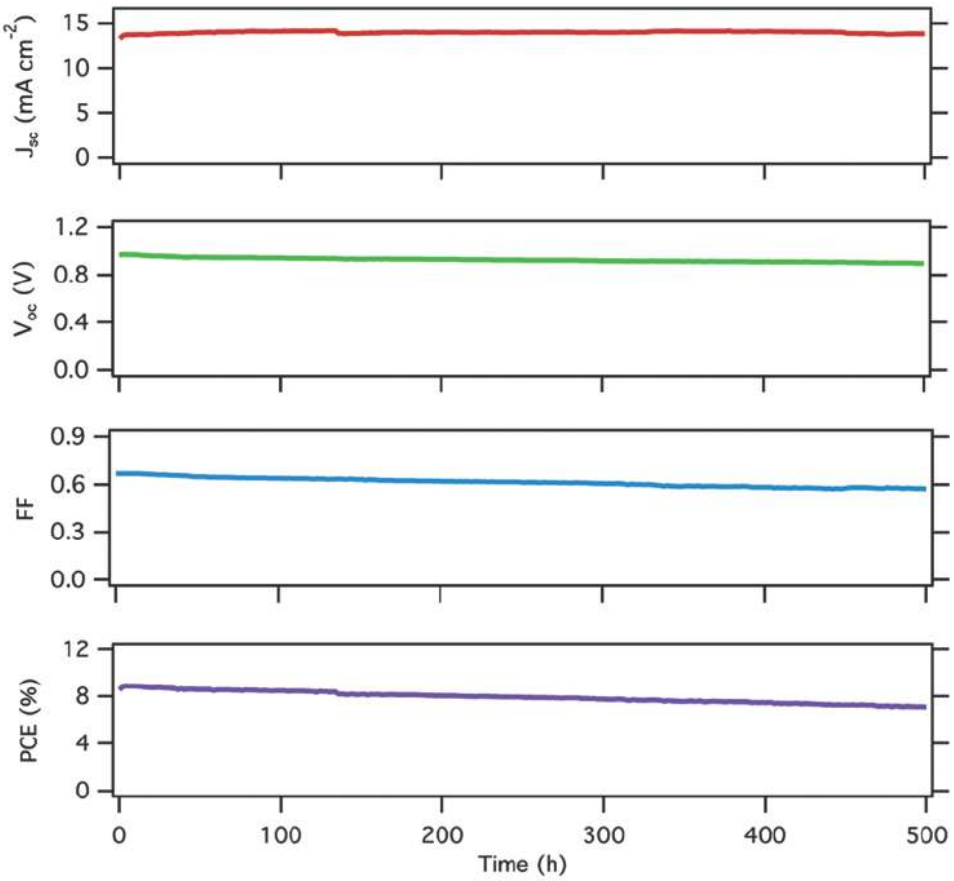

Fig. 6: Light soaking tests of regular PSCs under visible light (white LED light).

Reproduced with permission [16] Copyright 2013, Nature Publishing Group.

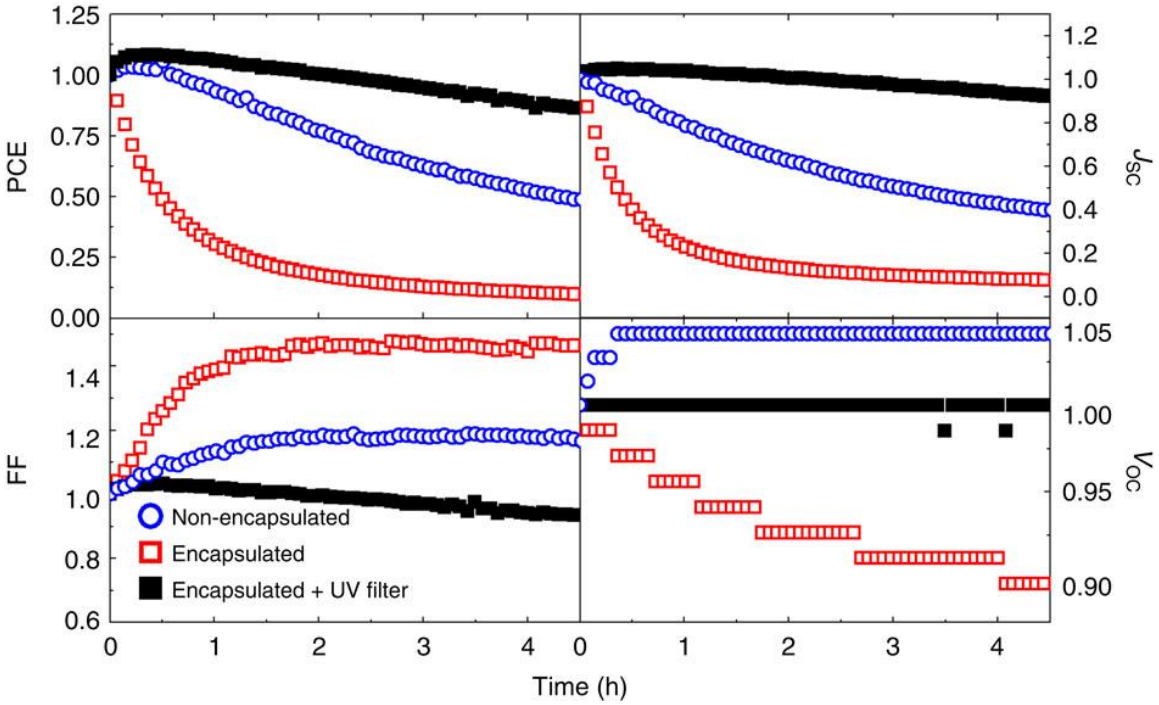

Fig. 7: Light soaking tests of regular PSCs under A.M. 1.5G 1 Sun light intensity (with and without UV filters). Reproduced with permission [192] Copyright 2013, Nature Publishing Group.

.

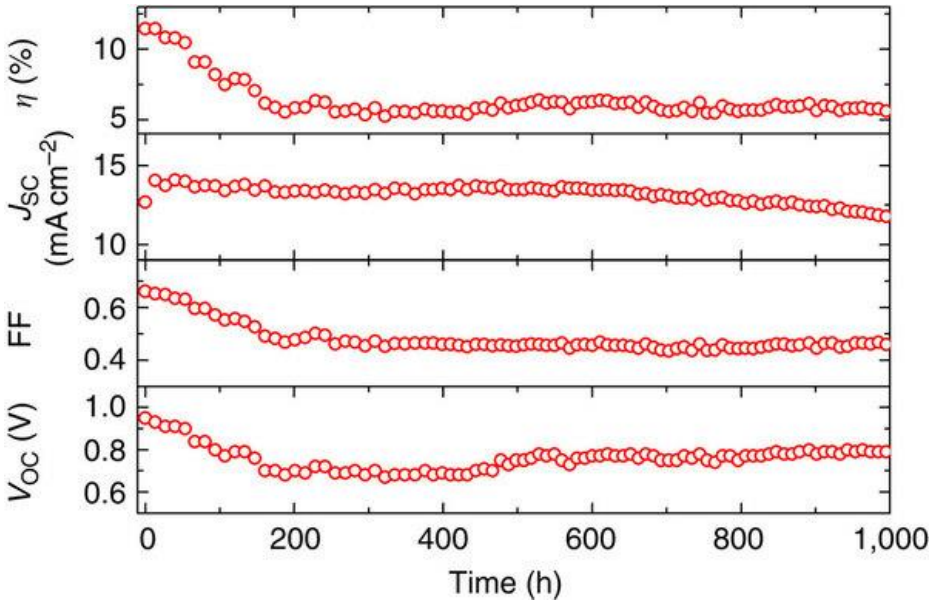

Fig. 8: Light soaking tests of MSSC PSCs under AM 1.5G 1 Sun light intensity at open circuit condition. Reproduced with permission [192] Copyright 2013, Nature Publishing Group.

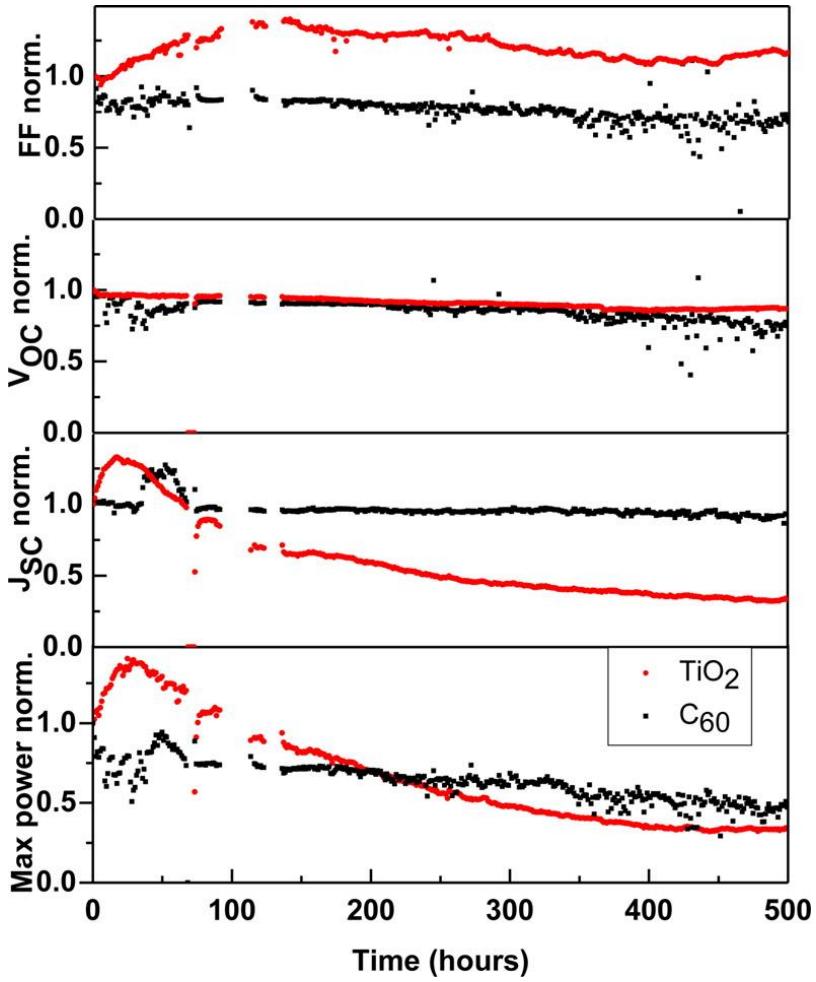

Fig. 9: Light soaking tests of MSSC PSCs under AM 1.5G 1 Sun light intensity at maximum power point condition. Reproduced with permission [193] Copyright 2015, American Chemical Society.

It is worth mentioning that application of UV filters has certain disadvantages. First, UV filters are susceptible of photo-bleaching for an operation of 25 years. Secondly, use of UV filters increase the cost of PSCs. But the biggest disadvantage of using UV filters is that it decrease the photovoltaic performance of the cells. Although the stability of PSCs is gradually improving, much work need to be done to stabilize the cell at high temperature (~ 85^{o}C) under operating condition. The most challenging test for PSCs would be to pass light soaking test at high temperature i.e. 85^{o}C, especially in damp conditions RH 85%.

6.4 Sealing issues

The most important purpose of sealing is to prevent moisture intrusion into the PSC, since there is no doubt about the detrimental role of moisture on the stability of PSCs. Especially for lead free PSCs where Sn has been used as alternate metal cation, the oxygen ingress is even more crucial to the device stability. It is also worth mentioning that the moisture resistant layers discussed in previous section may be partly or fully successful is preventing moisture intrusion into the cell effectively, these layers are not able to block oxygen invasion into the cell. Therefore, sealing of the cell is very crucial for the PSCs, especially for the lead free PCSs.

One common method of encapsulation is using cavity glass and a UV-curable resin. The PSCs based on $MAPbI_{3-x}Cl_x$ perovskite materials sealed with this method has shown reasonable long term stability in ambient atmosphere by retaining 90% of their initial performance for almost 2 months [126]. In another study UV activated glue is used in cells which demonstrated high stable (less than 10% loss in performance after 1000 h in AM 1.5

G 100 mW/cm^2) and efficient (η > 15%) PSCs [78]. Another successful method that has been used in organic photovoltaic (OPV) and can be equally effective for PSCs, is complete glass based sealing [194]. Although this glass based sealing effectively prevent moisture and oxygen penetration, the disadvantage of this sealing method is their unsuitability for flexible PSCs. Similar encapsulation methods used in OPV involving attachment of the glass or metal to the device using a slow permeation adhesive material [195], [196] are suitable for encapsulating rigid PSCs application. For flexible PSCs encapsulation, lamination of plastic films of the devices is an option. Depending on the composition of the laminates used, the degree of oxygen and moisture penetration vary quite much. Encapsulations of PSC modules with glass covers and thermoplastic sealants have already been reported [197].

6.5 Cross-line between performance and stability limiting factors

We would like to highlight that in a stability study it is important to keep track of performance limiting factors. The performance of a cell which is expressed in terms of performance parameters including short-circuit current density (J_{sc}), open circuit voltage (V_{oc}), fill factor (FF) and efficiency (η) depends on many different processes, for example, light absorption, charge separation, charge carriers transport mechanisms in different layers. Degradation in more than one process, can have same effect on the performance parameters. For instance, consider a hypothetical case where degradation of J_{sc} is suspected to be either due to degradation in perovskite film which reduces the photocurrent generation or due to degradation in HTM which limits the holes transport. If the

photocurrent is limited by the decreased transport in the HTM instead of the absorption, charges separation and transport in the perovskite film, the achieved stability is not a sufficient proof to conclude that the perovskite film was stable during the test. For instance, suppose that a poorly performing HTM suppresses the J_{sc} to 50% of the value obtained with a higher performance HTM, due to limited transport in the HTM. If J_{sc} stays constant, we cannot conclude stability of perovskite film since J_{sc} is not limited by performance of perovskite film, but the performance of HTM layer. Certain amount of degradation can occur in perovskite film which may have affected 50% of the J_{sc}, but now remained undetected. In general, this is just an example of the fact that investigation of stability in terms of η, J_{sc}, FF, V_{oc}, is sensitive to changes in only those properties that in the practical case affect these parameters. In this case J_{sc} was not sensitive to the degradation in perovskite film.

7. Environmental assessment

PSC technology often face criticism due to the use of toxic materials. Toxicity of lead [198], [199], [200], [201] together with usage of organometallic halide in PSCs, raises concerns about the human exposure during device manufacturing and also their impact on the environment in case of encapsulation failure [202] or during recycling of the materials. Several studies [199], [203], [204] have been conducted on acute and chronic lead exposure of humans, and it was found that lowest exposure level resulted in detectable effects, bio-accumulation and poisoning. Moreover, other toxic chemicals used in PSCs, especially iodine [205], [206] and methylamine

[207], [208], [209], can cause health hazards too if not handled properly. It is worth mentioning that one of the main route of volatile nanoparticles of $MAPbI_3$ to the human body is through inhalation [210]. Then, this airborne material can be deposited in the respiratory path (nose, bronchi and lungs) and get in contact with epithelial cells. Since the material is soluble in body fluids, it can reach brain through the blood or olfactory nerves [198], [199], [204], [211], [212].

Recently Benmessaoud et al. [204] performed a study on the most widely used perovskite material $MAPbI_3$. Their study provided detail insights into the cellular mechanisms through which $MAPbI_3$ can be potentially bio-accumulated in the body and cause serious health hazards in the long run. According to their study, the effect of $MAPbI_3$ is cell-type dependent. Exposure of $MAPbI_3$ to primary neurons and neuroblastoma cells, caused massive apoptotic cell deaths. On the other hand, exposure to epithelial cells dramatically affected their kinetics proliferation, their metabolic activity and cellular morphology without inducing noticeable cell death [204]. Therefore, it is clear that $MAPbI_3$ may have serious health effects.

Furthermore, since its degradation products are water soluble, it can penetrate through the human skin [213], [214]. Hence, we encourage researchers working on PSCs to be aware of the possible health hazards and take proper precautions accordingly. Furthermore, there is a need to improve the encapsulation of the PSC modules to avoid environmental hazards due to encapsulation failures. Finally, recycling of PSCs need to be studied in more detail.

8. Summary and prospects

Long term device stability is one of the most important challenge for the emerging PSC technology. Although encouraging aging results have been reported at milder or controlled environmental conditions, still there is a long way to go to meet stability standards of thin film PV technology (IEC 61646) and crystalline silicon PV technology (IEC 61215). Especially, no promising results have been reported yet for heat damp test (85ºC, 85 RH) and light soaking tests at 85ºC. Both the materials and their preparation methods have been found to influence the device stability. Certain structural configurations employing moisture blocking layers have shown promising stability results. In order to improve the stability of PSCs, it is inevitable to understand the degradation mechanisms in the device. Novel materials are required to test in the device for improved stability. Furthermore, conventional PV measurements need to be coupled with techniques giving chemical and structural information, to understand the origin of degradation. Systematic long term aging tests need to be performed to find out the conditions at which degradation reactions are originated or accelerated. Finally, alternative environmentally friendly materials are required to replace lead based PSCs.

Acknowledgements

The authors thank Academy of Finland (Grant No. 13282962 and 13287204) and National Natural Science Foundation of China (Grant No. 11374090 and 51372075) for their financial support.

References

[1] D. Bi, C. Yi, J. Luo, J.-D. Décoppet, F. Zhang, S.M. Zakeeruddin, X. Li, A. Hagfeldt, M. Grätzel, Polymer-templated nucleation and crystal growth of perovskite films for solar cells with efficiency greater than 21%, Nat. Energy. 1 (2016) 16142. doi:10.1038/nenergy.2016.142.

[2] D.-Y. Son, J.-W. Lee, Y.J. Choi, I.-H. Jang, S. Lee, P.J. Yoo, H. Shin, N. Ahn, M. Choi, D. Kim, N.-G. Park, Self-formed grain boundary healing layer for highly efficient CH3 NH3 PbI3 perovskite solar cells, Nat. Energy. 1 (2016) 16081. doi:10.1038/nenergy.2016.81.

[3] N.J. Jeon, Compositional engineering of perovskite materials for high-performance solar cells, Nature. 517 (2015) 476–480. doi:10.1038/nature14133.

[4] W.S. Yang, High-performance photovoltaic perovskite layers fabricated through intramolecular exchange, Science. 348 (2015) 1234–1237.

[5] S. Albrecht, M. Saliba, J.P.C. Baena, F. Lang, L. Kegelmann, M. Mews, L. Steier, A. Abate, J. Rappich, L. Korte, R. Schlatmann, M.K. Nazeeruddin, A. Hagfeldt, M. Grätzel, B. Rech, Monolithic perovskite/silicon-heterojunction tandem solar cells processed at low temperature, Energy Environ. Sci. 9 (2016) 81–88.

[6] F. Fu, T. Feurer, T. Jäger, E. Avancini, B. Bissig, S. Yoon, S. Buecheler, A.N. Tiwari, Low-temperature-processed efficient semi-transparent planar perovskite solar cells for bifacial and tandem applications, Nat. Commun. 6 (2015) 8932.

[7] C.R. Osterwald, T.J. McMahon, History of Accelerated and Qualification Testing of Terrestrial Photovoltaic Modules: A Literature Review, Progr. Photovolt.: Res. Appl. 17 (2009) 11–33.

[8] D.B. Mitzi, Synthesis, crystal structure, and optical and thermal properties of (C4H9NH3)2M14(M=Ge,Sn,Pb), Chemistry of Materials. 8 (1996) 791–800.

[9] E. Edri, S. Kirmayer, D. Cahen, G. Hodes, High open-circuit voltage solar cells based on organic–inorganic lead bromide perovskite, J. Phys. Chem. Lett. 4 (2013) 897–902.

[10] C. Eames, Ionic transport in hybrid lead iodide perovskite solar cells, Nature Communications. 6 (2015). doi:10.1038/ncomms8497.

[11] S.D. Stranks, G.E. Eperon, G. Grancini, C. Menelaou, M.J. Alcocer, T. Leijtens, L.M. Herz, A. Petrozza, H.J. Snaith, Electron-hole diffusion lengths exceeding 1 micrometer in an organometal trihalide perovskite absorber, Science. 342 (2013) 341–344.

[12] S. Ameen, M.S. Akhtar, H.-K. Seo, M.K. Nazeeruddin, H.-S. Shin, Exclusion of metal oxide by an RF sputtered Ti layer in flexible perovskite solar cells: energetic interface between a Ti layer and an organic charge transporting layer, Dalton Trans. 44 (2015) 6439–6448.

[13] Q. Dong, Y. Fang, Y. Shao, P. Mulligan, J. Qiu, L. Cao, J. Huang, Electron-hole diffusion lengths> 175 μm in solution-grown CH3NH3PbI3 single crystals, Science. 347 (2015) 967–970.

[14] T. Baikie, Y. Fang, J.M. Kadro, M. Schreyer, F. Wei, S.G. Mhaisalkar, M. Graetzel, T.J. White, Synthesis and crystal chemistry of the hybrid perovskite (CH 3 NH 3) PbI 3 for solid-state sensitised solar cell applications, J. Mater. Chem. A. 1 (2013) 5628–5641.

[15] K.M. Boopathi, M. Ramesh, P. Perumal, Y.-C. Huang, C.-S. Tsao, Y.-F. Chen, C.-H. Lee, C.-W. Chu, Preparation of metal halide perovskite solar cells through a liquid droplet assisted method, J. Mater. Chem. A. 3 (2015) 9257–9263.
[16] J. Burschka, N. Pellet, S.-J. Moon, R. Humphry-Baker, P. Gao, M.K. Nazeeruddin, M. Grätzel, Sequential deposition as a route to high-performance perovskite-sensitized solar cells, Nature. 499 (2013) 316–319.
[17] S. Sun, The origin of high efficiency in low-temperature solution-processable bilayer organometal halide hybrid solar cells, Energy Environ. Sci. 7 (2014) 399–407.
[18] H. Hu, D. Wang, Y. Zhou, J. Zhang, S. Lv, S. Pang, X. Chen, Z. Liu, N.P. Padture, G. Cui, Vapour-based processing of hole-conductor-free CH 3 NH 3 PbI 3 perovskite/C 60 fullerene planar solar cells, RSC Adv. 4 (2014) 28964–28967.
[19] A. Binek, F.C. Hanusch, P. Docampo, T. Bein, Stabilization of the Trigonal High-Temperature Phase of Formamidinium Lead Iodide, J. Phys. Chem. Lett. 6 (2015) 1249–1253.
[20] F. Hao, Anomalous Band Gap Behavior in Mixed Sn and Pb Perovskites Enables Broadening of Absorption Spectrum in Solar Cells, J. Am. Chem. Soc. 136 (22) (2014) 8094–8099.
[21] B. Conings, L. Baeten, C. De Dobbelaere, J. D'Haen, J. Manca, H. Boyen, Perovskite-Based Hybrid Solar Cells Exceeding 10% Efficiency with High Reproducibility Using a Thin Film Sandwich Approach, Adv. Mater. 26 (2014) 2041–2046.
[22] J.M. Ball, M.M. Lee, A. Hey, H.J. Snaith, Low-temperature processed meso-superstructured to thin-film perovskite solar cells, Energy Environ. Sci. 6 (2013) 1739–1743.
[23] M.A. Green, A. Ho-Baillie, H.J. Snaith, The emergence of perovskite solar cells, Nat. Photonics. 8 (2014) 506–514.
[24] A. Abate, M. Planells, D.J. Hollman, V. Barthi, S. Chand, H.J. Snaith, N. Robertson, Hole-transport materials with greatly-differing redox potentials give efficient TiO 2–[CH 3 NH 3][PbX 3] perovskite solar cells, Phys. Chem. Chem. Phys. 17 (2015) 2335–2338.
[25] C.-Y. Chang, C.-Y. Chu, Y.-C. Huang, C.-W. Huang, S.-Y. Chang, C.-A. Chen, C.-Y. Chao, W.-F. Su, Tuning perovskite morphology by polymer additive for high efficiency solar cell, ACS Appl. Mater. Interfaces. 7 (2015) 4955–4961.
[26] B. Conings, L. Baeten, T. Jacobs, R. Dera, J. D'Haen, J. Manca, H.-G. Boyen, An easy-to-fabricate low-temperature TiO2 electron collection layer for high efficiency planar heterojunction perovskite solar cells, APL Mater. 2 (2014) 081505.
[27] K.W. Tan, D.T. Moore, M. Saliba, H. Sai, L.A. Estroff, T. Hanrath, H.J. Snaith, U. Wiesner, Thermally induced structural evolution and performance of mesoporous block copolymer-directed alumina perovskite solar cells, ACS Nano. 8 (2014) 4730–4739.
[28] J.H. Noh, S.H. Im, J.H. Heo, T.N. Mandal, S.I. Seok, Chemical management for colorful, efficient, and stable inorganic–organic hybrid nanostructured solar cells, Nano Lett. 13 (2013) 1764–1769.

[29] A. Sadhanala, Blue-Green Color Tunable Solution Processable Organolead Chloride–Bromide Mixed Halide Perovskites for Optoelectronic Applications, Nano Letters. 15(9) (2015) 6095–6101.
[30] Y. Ye, Nature of the band gap of halide perovskites ABX3 (A = CH3NH3, Cs; B = Sn, Pb; X = Cl, Br, I): First-principles calculations*, Chin. Phys. B. 24 (11) (2015) 116302.
[31] T. Leijtens, G.E. Eperon, N.K. Noel, S.N. Habisreutinger, A. Petrozza, H.J. Snaith, Stability of Metal Halide Perovskite Solar Cells, Adv. Energy Mater. 5 (2015) 1500963.
[32] T. Leijtens, Electronic Properties of Meso-Superstructured and Planar Organometal Halide Perovskite Films: Charge Trapping, Photodoping, and Carrier Mobility, ACS Nano. 8 (7) (2014) 7147–7155.
[33] H. Zhou, Q. Chen, G. Li, S. Luo, T. Song, H.-S. Duan, Z. Hong, J. You, Y. Liu, Y. Yang, Interface engineering of highly efficient perovskite solar cells, Science. 345 (2014) 542–546.
[34] Z. Yu, Recent Progress on Hole-Transporting Materials for Emerging Organometal Halide Perovskite Solar Cells, Adv. Energy Mater. 5 (2015) 1500213.
[35] N.J. Jeon, H.G. Lee, Y.C. Kim, J. Seo, J.H. Noh, J. Lee, S.I. Seok, o-Methoxy substituents in spiro-OMeTAD for efficient inorganic–organic hybrid perovskite solar cells, J. Am. Chem. Soc. 136 (2014) 7837–7840.
[36] H. Doi, Star-shaped hole transporting materials with a triazine unit for efficient perovskite solar cells, Chem. Commun. 50 (2014) 10971–10974.
[37] H. Choi, Efficient Perovskite Solar Cells with 13.63 % Efficiency Based on Planar Triphenylamine Hole Conductors, Chem. Eur. J. 20 (2014) 10894–10899.
[38] H. Choi, Efficient star-shaped hole transporting materials with diphenylethenyl side arms for an efficient perovskite solar cell, J. Mater. Chem. A. 2 (2014) 19136–19140.
[39] N.J. Jeon, J. Lee, J.H. Noh, M.K. Nazeeruddin, M. Grätzel, S.I. Seok, Efficient inorganic–organic hybrid perovskite solar cells based on pyrene arylamine derivatives as hole-transporting materials, J. Am. Chem. Soc. 135 (2013) 19087–19090.
[40] N.J. Jeon, J.H. Noh, Y.C. Kim, W.S. Yang, S. Ryu, S.I. Seok, Solvent engineering for high-performance inorganic–organic hybrid perovskite solar cells, Nat. Mater. (2014).
[41] Z. Zhu, Polyfluorene Derivatives are High-Performance Organic Hole-Transporting Materials for Inorganic− Organic Hybrid Perovskite Solar Cells, Adv. Funct. Mater. 24 (2014) 7357–7365.
[42] M. Cheng, B. Xu, C. Chen, X. Yang, F. Zhang, Q. Tan, Y. Hua, L. Kloo, L. Sun, Phenoxazine-Based Small Molecule Material for Efficient Perovskite Solar Cells and Bulk Heterojunction Organic Solar Cells, Adv. Energy Mater. 5 (2015).
[43] S.D. Sung, 14.8% perovskite solar cells employing carbazole derivatives as hole transporting materials, Chem. Commun. 50 (2014) 14161–14163.
[44] Y. Song, Energy level tuning of TPB-based hole-transporting materials for highly efficient perovskite solar cells, Chem. Commun. 50 (2014) 15239–15242.

[45] P. Qin, Perovskite solar cells with 12.8% efficiency by using conjugated quinolizino acridine based hole transporting material, J. Am. Chem. Soc. 136 (2014) 8516–8519.
[46] H. Li, A simple 3,4-ethylenedioxythiophene based hole-transporting material for perovskite solar cells, Angew. Chem. Int. Ed. 53 (2014) 4085–4088.
[47] H. Li, Hole-transporting small molecules based on thiophene cores for high efficiency perovskite solar cells, ChemSusChem. 7 (2014) 3420–3425.
[48] P. Qin, Inorganic hole conductor-based lead halide perovskite solar cells with 12.4% conversion efficiency, Nat. Commun. 5 (2014) 3834.
[49] S. Ito, S. Tanaka, H. Nishino, Lead-Halide Perovskite Solar Cells by CH3NH3I Dripping on PbI2–CH3NH3I–DMSO Precursor Layer for Planar and Porous Structures Using CuSCN Hole-Transporting Material, J. Phys. Chem. Lett. 6 (2015) 881–886.
[50] K. Aitola, Carbon nanotube-based hybrid hole-transporting material and selective contact for high efficiency perovskite solar cells, Energy Environ. Sci. accepted (2016). doi:10.1039/C5EE03394B.
[51] J.H. Heo, S.H. Im, J.H. Noh, T.N. Mandal, C.-S. Lim, J.A. Chang, Y.H. Lee, H. Kim, A. Sarkar, M.K. Nazeeruddin, Efficient inorganic-organic hybrid heterojunction solar cells containing perovskite compound and polymeric hole conductors, Nat. Photonics. 7 (2013) 486–491.
[52] E.J. Juarez-Perez, M. Wuβler, F. Fabregat-Santiago, K. Lakus-Wollny, E. Mankel, T. Mayer, W. Jaegermann, I. Mora-Sero, Role of the selective contacts in the performance of lead halide perovskite solar cells, J. Phys. Chem. Lett. 5 (2014) 680–685.
[53] Q. Chen, H. Zhou, Z. Hong, S. Luo, H.-S. Duan, H.-H. Wang, Y. Liu, G. Li, Y. Yang, Planar heterojunction perovskite solar cells via vapor-assisted solution process, J. Am. Chem. Soc. 136 (2013) 622–625.
[54] X. Xu, Z. Liu, Z. Zuo, M. Zhang, Z. Zhao, Y. Shen, H. Zhou, Q. Chen, Y. Yang, M. Wang, Hole Selective NiO Contact for Efficient Perovskite Solar Cells with Carbon Electrode, Nano Lett. 15 (2015) 2402–2408.
[55] X. Yin, High efficiency hysteresis-less inverted planar heterojunction perovskite solar cells with a solution-derived NiOx hole contact layer, J. Mater. Chem. A. 3 (2015) 24495–24503.
[56] M. Batmunkh, C.J. Shearer, M.J. Biggs, J.G. Shapter, Nanocarbons for mesoscopic perovskite solar cells, J. Mater. Chem. A. 3 (2015) 9020–9031.
[57] F. Zhang, Engineering of hole-selective contact for low temperature-processed carbon counter electrode-based perovskite solar cells, J. Mater. Chem. A. 3 (2015) 24272–24280.
[58] S.A. Kulkarni, T. Baikie, P.P. Boix, N. Yantara, N. Mathews, S. Mhaisalkar, Band-gap tuning of lead halide perovskites using a sequential deposition process, J. Mater. Chem. A. 2 (2014) 9221–9225.
[59] Y. Han, S. Meyer, Y. Dkhissi, K. Weber, J.M. Pringle, U. Bach, L. Spiccia, Y.-B. Cheng, Degradation observations of encapsulated planar CH 3 NH 3 PbI 3 perovskite solar cells at high temperatures and humidity, J. Mater. Chem. A. 3 (2015) 8139–8147.

[60] Y. Chen, J. Peng, D. Su, X. Chen, Z. Liang, Efficient and Balanced Charge Transport Revealed in Planar Perovskite Solar Cells, ACS Appl. Mater. Interfaces. 7 (2015) 4471–4475.
[61] P. Docampo, J.M. Ball, M. Darwich, G.E. Eperon, H.J. Snaith, Efficient organometal trihalide perovskite planar-heterojunction solar cells on flexible polymer substrates, Nat. Commun. 4 (2013).
[62] J. Jeng, Y. Chiang, M. Lee, S. Peng, T. Guo, P. Chen, T. Wen, CH3NH3PbI3 Perovskite/Fullerene Planar-Heterojunction Hybrid Solar Cells, Adv. Mater. 25 (2013) 3727–3732.
[63] L. Gil-Escrig, G. Longo, A. Pertegás, C. Roldán-Carmona, A. Soriano, M. Sessolo, H.J. Bolink, Efficient photovoltaic and electroluminescent perovskite devices, Chem. Commun. 51 (2015) 569–571.
[64] M.H. Kumar, N. Yantara, S. Dharani, M. Graetzel, S. Mhaisalkar, P.P. Boix, N. Mathews, Flexible, low-temperature, solution processed ZnO-based perovskite solid state solar cells, Chem. Commun. 49 (2013) 11089–11091.
[65] G. Hodes, D. Cahen, Photovoltaics: Perovskite cells roll forward, Nat. Photonics. 8 (2014) 87–88.
[66] Y. Li, L. Meng, Y. Yang, Y.G. Xu, Z. Hong, Q. Chen, J. You, G. Li, Y. Yang, Y. Li, High-efficiency robust perovskite solar cells on ultrathin flexible substrates, Nat. Commun. 7 (2016) 10214.
[67] S.S. Shin, W.S. Yang, J.H. Noh, J.H. Suk, N.J. Jeon, J.H. Park, W.M. Seong, S.I. Seok, High-performance flexible perovskite solar cells exploiting Zn2SnO4 prepared in solution below 100 °C, Nat Commun. 6 (2015) 7410.
[68] M. Lee, Y. Jo, D.S. Kim, Y. Jun, Flexible organo-metal halide perovskite solar cells on a Ti metal substrate, J. Mater. Chem. A. 3 (2015) 4129–4133.
[69] J. Troughton, D. Bryant, K. Wojciechowski, M.J. Carnie, H. Snaith, D.A. Worsley, T.M. Watson, Highly efficient, flexible, indium-free perovskite solar cells employing metallic substrates, J. Mater. Chem. A. 3 (2015) 9141–9145.
[70] L. Qiu, J. Deng, X. Lu, Z. Yang, H. Peng, Integrating Perovskite Solar Cells into a Flexible Fiber, Angew. Chem. Int. Ed. 53 (2014) 10425–10428.
[71] K. Wojciechowski, M. Saliba, T. Leijtens, A. Abate, H.J. Snaith, Sub-150 C processed meso-superstructured perovskite solar cells with enhanced efficiency, Energy Environ. Sci. 7 (2014) 1142–1147.
[72] W. Ke, G. Fang, J. Wan, H. Tao, Q. Liu, L. Xiong, P. Qin, J. Wang, H. Lei, G. Yang, Efficient hole-blocking layer-free planar halide perovskite thin-film solar cells, Nat. Commun. 6 (2015) 6700.
[73] G. Xing, N. Mathews, S. Sun, S.S. Lim, Y.M. Lam, M. Graetzel, S. Mhaisalkar, T.C. Sum, Long-Range Balanced Electronand Hole-Transport Lengths in Organic-Inorganic CH3NH3PbI3, 342 (2013) 344–347.
[74] E. Edri, S. Kirmayer, S. Mukhopadhyay, K. Gartsman, G. Hodes, D. Cahen, Elucidating the charge carrier separation and working mechanism of CH3NH3PbI3−xClx perovskite solar cells, Nat. Commun. 5 (2014).
[75] C.S. Ponseca Jr, Y. Tian, V. Sundström, I.G. Scheblykin, Excited state and charge-carrier dynamics in perovskite solar cell materials, Nanotechnology. 27 (2016) 082001.

[76] T.J. Savenije, C.S. Ponseca Jr, L. Kunneman, M. Abdellah, K. Zheng, Y. Tian, Q. Zhu, S.E. Canton, I.G. Scheblykin, T. Pullerits, Thermally activated exciton dissociation and recombination control the carrier dynamics in organometal halide perovskite, J. Phys. Chem. Lett. 5 (2014) 2189–2194.
[77] S. Ito, S. Tanaka, H. Vahlman, H. Nishino, K. Manabe, P. Lund, Carbon-Double-Bond-Free Printed Solar Cells from TiO2/CH3NH3PbI3/CuSCN/Au: Structural Control and Photoaging Effects, ChemPhysChem. 15 (2014) 1194–1200.
[78] W. Chen, Y. Wu, Y. Yue, J. Liu, W. Zhang, X. Yang, H. Chen, E. Bi, I. Ashraful, M. Grätzel, L. Han, Efficient and stable large-area perovskite solar cells with inorganic charge extraction layers, Science. 350 (2015) 944–948.
[79] F. Wang, H. Yu, H. Xu, N. Zhao, HPbI3: A New Precursor Compound for Highly Efficient Solution-Processed Perovskite Solar Cells, Adv. Funct. Mater. 25 (2015) 1120–1126.
[80] S. Kazim, M.K. Nazeeruddin, M. Grätzel, S. Ahmad, Perovskite as light harvester: a game changer in photovoltaics, Angew. Chem. Int. Ed. 53 (2014) 2812–2824.
[81] Y. Ma, L. Zheng, Y.-H. Chung, S. Chu, L. Xiao, Z. Chen, S. Wang, B. Qu, Q. Gong, Z. Wu, A highly efficient mesoscopic solar cell based on CH 3 NH 3 PbI 3− x Cl x fabricated via sequential solution deposition, Chem. Commun. 50 (2014) 12458–12461.
[82] L. Zheng, Y. Ma, S. Chu, S. Wang, B. Qu, L. Xiao, Z. Chen, Q. Gong, Z. Wu, X. Hou, Improved light absorption and charge transport for perovskite solar cells with rough interfaces by sequential deposition, Nanoscale. 6 (2014) 8171–8176.
[83] A. Mei, X. Li, L. Liu, Z. Ku, T. Liu, Y. Rong, M. Xu, M. Hu, J. Chen, Y. Yang, A hole-conductor–free, fully printable mesoscopic perovskite solar cell with high stability, Science. 345 (2014) 295–298.
[84] H. Chen, Z. Wei, X. Zheng, S. Yang, A scalable electrodeposition route to the low-cost, versatile and controllable fabrication of perovskite solar cells, Nano Energy. 15 (2015) 216–226.
[85] S. Das, B. Yang, G. Gu, P.C. Joshi, I.N. Ivanov, C.M. Rouleau, T. Aytug, D.B. Geohegan, K. Xiao, High-Performance Flexible Perovskite Solar Cells by Using a Combination of Ultrasonic Spray-Coating and Low Thermal Budget Photonic Curing, ACS Photonics. 2 (2015) 680–686.
[86] K. Hwang, Y. Jung, Y. Heo, F.H. Scholes, S.E. Watkins, J. Subbiah, D.J. Jones, D.Y. Kim, D. Vak, Toward large scale roll-to-roll production of fully printed perovskite solar cells., Adv. Mater. 27 (2015) 1241–1247.
[87] M. Yang, Y. Zhou, Y. Zeng, S.S. Jiang, N.P. Padture, K. Zhu, Square-Centimeter Solution-Processed Planar CH3NH3PbI3 Perovskite Solar Cells with Efficiency Exceeding 15%, Adv. Mater. 27 (2015) 6363–6370.
[88] M.M. Tavakoli, L. Gu, Y. Gao, C. Reckmeier, J. He, A.L. Rogach, Y. Yao, Z. Fan, Fabrication of efficient planar perovskite solar cells using a one-step chemical vapor deposition method, Scientific Reports. 5 (2015) 14083.
[89] M. Liu, M.B. Johnston, H.J. Snaith, Efficient planar heterojunction perovskite solar cells by vapour deposition, Nature. 501 (2013) 395–398.

[90] Q. Ma, S. Huang, X. Wen, M.A. Green, Baillie, Hole Transport Layer Free Inorganic CsPbIBr2 Perovskite Solar Cell by Dual Source Thermal Evaporation Authors, Adv. Energy Mater. 6 (2016) 1502202.
[91] C.W. Chen, H.W. Kang, S.Y. Hsiao, P.F. Yang, K.M. Chiang, H.W. Lin, Efficient and uniform planar-type perovskite solar cells by simple sequential vacuum deposition., Adv. Mater. 26 (2014) 6647–6652.
[92] H. Back, J. Kim, G. Kim, T.K. Kim, H. Kang, J. Kong, S.H. Lee, K. Lee, Interfacial modification of hole transport layers for efficient large-area perovskite solar cells achieved via blade-coating, Sol. Energy Mater. Sol. Cells. 144 (2016) 309–315.
[93] K. Cao, Z. Zuo, J. Cui, Y. Shen, T. Moehl, S.M. Zakeeruddin, M. Grätzel, M. Wang, Efficient screen printed perovskite solar cells based on mesoscopic TiO2/Al2O3/NiO/carbon architecture, Nano Energy. 17 (2015) 171–179.
[94] S.G. Li, K.J. Jiang, M.J. Su, X.P. Cui, J.H. Huang, Q.Q. Zhang, X.Q. Zhou, L.M. Yang, Y.L. Song, Inkjet printing of CH3NH3PbI3 on a mesoscopic TiO2 film for highly efficient perovskite solar cells, J. Mater. Chem. A. 3 (2015) 9092–9097.
[95] X. Li, M. Tschumi, H. Han, S.S. Babkair, R.A. Alzubaydi, A.A. Ansari, S.S. Habib, M.K. Nazeeruddin, S.M. Zakeeruddin, M. Grätzel, Outdoor Performance and Stability under Elevated Temperatures and Long-Term Light Soaking of Triple-Layer Mesoporous Perovskite Photovoltaics, Energy Technol. 3 (2015) 551 – 555.
[96] J.-H. Im, J. Luo, M. Franckevicius, N. Pellet, P. Gao, T. Moehl, S.M. Zakeeruddin, M.K. Nazeeruddin, M. Grätzel, N.-G. Park, Nanowire Perovskite Solar Cell, Nano Lett. 15 (2015) 2120–2126.
[97] E. Horváth, M. Spina, Z. Szekrényes, K. Kamarás, R. Gaal, D. Gachet, L. Forró, Nanowires of Methylammonium Lead Iodide (CH3NH3PbI3) Prepared by Low Temperature Solution-Mediated Crystallization, Nano Lett. 14 (2014) 6761–6766.
[98] Y. Wu, X. Yang, H. Chen, K. Zhang, C. Qin, J. Liu, W. Peng, A. Islam, E. Bi, F. Ye, Highly compact TiO2 layer for efficient hole-blocking in perovskite solar cells, Appl. Phys. Express. 7 (2014) 052301.
[99] C. Jiang, S.L. Lim, W.P. Goh, F.X. Wei, J. Zhang, Improvement of CH3NH3PbI3 Formation for Efficient and Better Reproducible Mesoscopic Perovskite Solar Cells, ACS Appl. Mater. Interfaces. 7 (2015) 24726−24732.
[100] J. Kim, G. Kim, T.K. Kim, S. Kwon, H. Back, J. Lee, S.H. Lee, H. Kang, K. Lee, Efficient planar-heterojunction perovskite solar cells achieved via interfacial modification of a sol–gel ZnO electron collection layer, J. Mater. Chem. A. 2 (2014) 17291–17296.
[101] Z. Zhu, Y. Bai, T. Zhang, Z. Liu, X. Long, Z. Wei, L. Zhang, J. Wang, F. Fan, S. Yang, High-performance hole-extraction layer of sol-gel-processed NiO nanocrystals for inverted planar perovskite solar cells., Angew. Chem. Int. Ed. 53 (2014) 12571–12575.
[102] H.-S. Kim, J.-W. Lee, N. Yantara, P.P. Boix, S.A. Kulkarni, S. Mhaisalkar, M. Grätzel, N.-G. Park, High efficiency solid-state sensitized solar cell-based on submicrometer rutile TiO2 nanorod and CH3NH3PbI3 perovskite sensitizer, Nano Lett. 13 (2013) 2412–2417.

[103] K. Manseki, T. Ikeya, A. Tamura, T. Ban, T. Sugiura, T. Yoshida, Mg-doped TiO 2 nanorods improving open-circuit voltages of ammonium lead halide perovskite solar cells, RSC Adv. 4 (2014) 9652–9655.
[104] M. Yang, R. Guo, K. Kadel, Y. Liu, K. O'Shea, R. Bone, X. Wang, J. He, W. Li, Improved charge transport of Nb-doped TiO 2 nanorods in methylammonium lead iodide bromide perovskite solar cells, J. Mater. Chem. A. 2 (2014) 19616–19622.
[105] P. Qin, A.L. Domanski, A.K. Chandiran, R. Berger, H.-J. Butt, M.I. Dar, T. Moehl, N. Tetreault, P. Gao, S. Ahmad, Yttrium-substituted nanocrystalline TiO 2 photoanodes for perovskite based heterojunction solar cells, Nanoscale. 6 (2014) 1508–1514.
[106] S. He, L. Qiu, X. Fang, G. Guan, P. Chen, Z. Zhang, H. Peng, Radically grown obelisk-like ZnO arrays for perovskite solar cell fibers and fabrics through a mild solution process, J. Mater. Chem. A. 3 (2015) 9406–9410.
[107] J. Zhang, P. Barboux, T. Pauporté, Electrochemical Design of Nanostructured ZnO Charge Carrier Layers for Efficient Solid-State Perovskite-Sensitized Solar Cells, Adv. Energy Mater. 4 (2014).
[108] M.M. Tavakoli, K. Tsui, Q. Zhang, J. He, Y. Yao, D. Li, Z. Fan, Highly Efficient Flexible Perovskite Solar Cells with Antireflection and Self-Cleaning Nanostructures, ACS Nano. 9 (2015) 10287–10295.
[109] J.T.-W. Wang, J.M. Ball, E.M. Barea, A. Abate, J.A. Alexander-Webber, J. Huang, M. Saliba, I. Mora-Sero, J. Bisquert, H.J. Snaith, Low-temperature processed electron collection layers of graphene/TiO2 nanocomposites in thin film perovskite solar cells, Nano Lett. 14 (2013) 724–730.
[110] C. Chen, F. Li, F. Wu, F. Tan, Y. Zhai, W. Zhang, Efficient perovskite solar cells based on low-temperature solution-processed (CH3NH3)PbI3 perovskite/CuInS2 planar heterojunctions, Nanoscale Res Lett. 9 (2014) 457.
[111] L.E. Polander, P. Pahner, M. Schwarze, M. Saalfrank, C. Koerner, K. Leo, Hole-transport material variation in fully vacuum deposited perovskite solar cells, APL Mater. 2 (2014) 081503.
[112] J. Huang, M. Wang, L. Ding, F. Igbari, X. Yao, Efficiency enhancement of MAPbIxCl3−x based perovskite solar cell by modifying the TiO2 interface with Silver Nanowires, Solar Energy. 130 (2016) 273–280.
[113] H. Hu, K. Yan, M. Peng, X. Yu, S. Chen, B. Chen, B. Dong, X. Gao, D. Zou, Fiber-shaped perovskite solar cells with 5.3% efficiency, J. Mater. Chem. A. 4 (2016) 3901–3906.
[114] C. Chen, Y. Cheng, Q. Dai, H. Song, Radio Frequency Magnetron Sputtering Deposition of TiO2 Thin Films and Their Perovskite Solar Cell Applications, Scientific Reports. 5 (2015) 17684.
[115] N. Chander, A.F. Khan, P.S. Chandrasekhar, E. Thouti, S.K. Swami, V. Dutta, V.K. Komarala, Reduced ultraviolet light induced degradation and enhanced light harvesting using YVO4:Eu3+ down-shifting nano-phosphor layer in organometal halide perovskite solar cells, Appl. Phys. Lett. 105 (2014) 033904.
[116] Y. Xiao, G. Han, Y. Li, M. Li, Y. Chang, J. Wu, Preparation of high performance perovskitesensitized nanoporous titanium dioxide photoanodes by in situ method for use in perovskite solar cells, J. Mater. Chem. A. 2 (2014) 16531.

[117] C.G. Wu, C.H. Chiang, Z.L. Tseng, M.K. Nazeeruddin, A. Hagfeldt, M. Grätzel, High efficiency stable inverted perovskite solar cells without current hysteresis, Energy Environ. Sci. 8 (2015) 2725–2733.
[118] T. Moehl, J.-H. Im, Y.H. Lee, K. Domanski, F. Giordano, S.M. Zakeeruddin, M.I. Dar, L.-P. Heiniger, M.K. Nazeeruddin, N.G. Park, M. Graetzel, Strong Photocurrent Amplification in Perovskite Solar Cells with a Porous TiO2 Blocking Layer under Reverse Bias, J. Phys. Chem. Lett. 5 (2014) 3931–3936.
[119] J.-H. Im, I.H. Jang, N. Pellet, M. Grätzel, N.G. Park, Growth of CH3NH3PbI3 cuboids with controlled size for high-efficiency perovskite solar cells, Nature Nanotechnology. 9 (2014) 927–932.
[120] M. Kaltenbrunner, Flexible high power-per-weight perovskite solar cells with chromium oxide–metal contacts for improved stability in air, Nature Materials. 14 (2015) 1032–1039.
[121] W. Qiu, T. Merckx, M. Jaysankar, M. Huerta, L. Rakocevic, W. Zhang, U.W. Paetzold, R. Gehlhaar, L. Froyen, J. Poortmans, D. Cheyns, H.J. Snaith, P. heremans, Pinhole-free perovskite films for efficient solar modules, 9 (2016) 484–489.
[122] H.J. Snaith, A. Abate, J.M. Ball, G.E. Eperon, T. Leijtens, N.K. Noel, S.D. Stranks, J.T.-W. Wang, K. Wojciechowski, W. Zhang, Anomalous hysteresis in perovskite solar cells, J. Phys. Chem. Lett. 5 (2014) 1511–1515.
[123] R.S. Sanchez, V. Gonzalez-Pedro, J.-W. Lee, N.-G. Park, Y.S. Kang, I. Mora-Sero, J. Bisquert, Slow dynamic processes in lead halide perovskite solar cells. Characteristic times and hysteresis, J. Phys. Chem. Lett. 5 (2014) 2357–2363.
[124] H.S. Kim, N.G. Park, Parameters affecting I–V hysteresis of CH3NH3PbI3 perovskite solar cells: effects of perovskite crystal size and mesoporous TiO2 layer, J. Phys. Chem. Lett. 5 (2014) 2927– 2934.
[125] E.L. Unger, E.T. Hoke, C.D. Bailie, W.H. Nguyen, A.R. Bowring, T. Heumuller, M.G. Christoforo, M.D. McGehee, Hysteresis and transient behavior in current–voltage measurements of hybrid-perovskite absorber solar cells, Energy Environ. Sci. 7 (2014) 3690–3698.
[126] N. Tripathi, M. Yanagida, Y. Shirai, T. Masuda, L. Han, K. Miyano, Hysteresis-free and highly stable perovskite solar cells produced via a chlorine-mediated interdiffusion method, J. Mater. Chem. A. 3 (2015) 12081–12088.
[127] J. Cao, Y.-M. Liu, X. Jing, J. Yin, J. Li, B. Xu, Y.-Z. Tan, N. Zheng, Well-Defined Thiolated Nanographene as Hole-Transporting Material for Efficient and Stable Perovskite Solar Cells, J. Am. Chem. Soc. 137 (2015) 10914–10917.
[128] D. Bi, G. Boschloo, S. Schwarzmuller, L. Yang, E.M.J. Johansson, A. Hagfeldt, Efficient and stable CH3NH3PbI3-sensitized ZnO nanorod array solid-state solar cells, Nanoscale. 5 (2013) 11686–11691.
[129] J. Song, J. Bian, E. Zheng, X.-F. Wang, W. Tian, T. Miyasaka, Efficient and Environmentally Stable Perovskite Solar Cells Based on ZnO Electron Collection Layer, Chem. Lett. 44 (2015) 610–612.
[130] J. Song, E. Zheng, J. Bian, X.-F. Wang, W. Tian, Y. Sanehira, T. Miyasaka, Low-temperature SnO2-based electron selective contact for efficient and stable perovskite solar cells, J. Mater. Chem. A. 3 (2015) 10837–10844.

[131] J. Liu, Y. Wu, C. Qin, X. Yang, T. Yasuda, A. Islam, K. Zhang, W. Peng, W. Chen, L. Han, A dopant-free hole-transporting material for efficient and stable perovskite solar cells, Energy Environ. Sci. (2014) 2963–2967.
[132] J. You, L. Meng, T.B. Song, T. Guo, Y.M. Yang, W.H. Chang, Z. Hong, H. Chen, H. Zhou, Q. Chen, Y. Liu, N.D. Marco, Y. Yang, Improved air stability of perovskite solar cells via solution-processed metal oxide transport layers, Nature nanotechnology. 11 (2016) 75–81.
[133] J.H. Kim, P.W. Liang, S.T. Williams, N. Cho, C. Chueh, M.S. Glaz, D.S. Ginger, A.K.-Y. Jen, High-Performance and Environmentally Stable Planar Heterojunction Perovskite Solar Cells Based on a Solution-Processed Copper-Doped Nickel Oxide Hole-Transporting Layer, Adv. Mater. 27 (2015) 695–701.
[134] Y.S. Kwon, J. Lim, H.J. Yun, Y.H. Kim, T. Park, A diketopyrrolopyrrole-containing hole transporting conjugated polymer for use in efficient stable organic–inorganic hybrid solar cells based on a perovskite, Energy Environ. Sci. 7 (2014) 1454–1460.
[135] S. Guarnera, A. Abate, W. Zhang, J.M. Foster, G. Richardson, A. Petrozza, H.J. Snaith, Improving the Long-Term Stability of Perovskite Solar Cells with a Porous Al2O3 Buffer Layer, J. Phys. Chem. Lett. 6 (2015) 432−437.
[136] X. Dong, X. Fang, M. Lv, B. Lin, S. Zhang, J. Ding, N. Yuan, Improvement of the humidity stability of organic–inorganic perovskite solar cells using ultrathin Al2O3 layers prepared by atomic layer deposition, J. Mater. Chem. A. 3 (2015) 5360–5367.
[137] G. Niu, W. Li, F. Meng, L. Wang, H. Dong, Y. Qiu, Study on the stability of CH 3 NH 3 PbI 3 films and the effect of post-modification by aluminum oxide in all-solid-state hybrid solar cells, J. Mater. Chem. A. 2 (2014) 705–710.
[138] H. Back, G. Kim, J. Kim, J. Kong, T.K. Kim, H. Kang, H. Kim, J. Lee, S. Lee, K. Lee, Achieving long-term stable perovskite solar cells via ion neutralization, Energy Environ. Sci. 9 (2016) 1258--1263.
[139] K. Miettunen, M.I. Asghar, X. Ruan, J. Halme, T. Saukkonen, P. Lund, Stabilization of metal counter electrodes for dye solar cells, J. Electroanal. Chem. 653 (2011) 93–99.
[140] K. Miettunen, M.I. Asghar, S. Mastroianni, J. Halme, P.R.F. Barnes, E. Rikkinen, B.C. O'Regan, P. Lund, Effect of molecular filtering and electrolyte composition on the spatial variation in performance of dye solar cells, J. Electroanal. Chem. 664 (2012) 63–72. doi:10.1016/j.jelechem.2011.10.012.
[141] X.A. Jeanbourquin, X. Li, C. Law, P.R.F. Barnes, R. Humphry-Baker, P. Lund, B.C. O'Regan, Rediscovering a key interface in dye-Sensitized Solar Cells: Guanidinium and Iodine Competition for Binding Sites at the dye/Electrolyte Surface, J. Am. Chem. Soc. 136 (2014) 7286–7294. doi:10.1021/ja411560s.
[142] W. Kylberg, F.A. Castro, P. Chabrecek, T. Geiger, J. Heier, P.G. Nicholson, F. Nuesch, E. Theocharous, U. Sonderegger, R. Hany, Spatially resolved photocurrent mapping of efficient organic solar cells fabricated on a woven mesh electrode, Progr. Photovolt.: Res. Appl. 21 (2013) 652–657.
[143] S. Aharon, A. Dymshits, A. Rotem, L. Etgar, Temperature dependence of hole conductor free formamidinium lead iodide perovskite based solar cells, J. Mater. Chem. A. 3 (2015) 9171–9178.

[144] M.G. Christoforo, E.T. Hoke, M.D. McGehee, E.L. Unger, Transient Response of Organo-Metal-Halide Solar Cells Analyzed by Time-Resolved Current-Voltage Measurements, Photonics. 2 (2015) 1101–1115.
[145] B. Macht, M. Turrion, A. Barkschat, P. Salvador, K. Ellmer, H. Tributsch, Patterns of efficiency and degradation in dye sensitization solar cells measured with imaging techniques, Sol. Energy Mater. Sol. Cells. 73 (2002) 163–173.
[146] M.I. Asghar, K. Miettunen, S. Mastroianni, J. Halme, H. Vahlman, P. Lund, In situ image processing method to investigate performance and stability of dye solar cells, Solar Energy. 86 (2012) 331–338. doi:10.1016/j.solener.2011.10.006.
[147] A.R. Andersen, J. Halme, T. Lund, M.I. Asghar, P.T. Nguyen, K. Miettunen, E. Kemppainen, O. Albrektsen, Charge Transport and Photocurrent Generation Characteristics in Dye Solar Cells Containing Thermally Degraded N719 Dye Molecules, J. Phys. Chem. C. 115 (2011) 15598–15606.
[148] Y. Zhao, J. Wei, H. Li, Y. Yan, W. Zhou, D. Yu, Q. Zhao, A polymer scaffold for self-healing perovskite solar cells, Nat. Commun. 7 (2016) 10228.
[149] H.-S. Ko, J.-W. Lee, N.-G. Park, 15.76% efficiency perovskite solar cells prepared under high relative humidity: importance of PbI 2 morphology in two-step deposition of CH 3 NH 3 PbI 3, J. Mater. Chem. A. 3 (2015) 8808–8815.
[150] Y. Zhou, A.L. Vasiliev, W. Wu, M. Yang, S. Pang, K. Zhu, N.P. Padture, Crystal Morphologies of Organolead Trihalide in Mesoscopic/Planar Perovskite Solar Cells, J. Phys. Chem. Lett. 6 (2015) 2292–2297.
[151] F. Matteocci, Y. Busby, J.J. Pireaux, G. Divitini, S. Cacovich, C. Ducati, A.D. Carlo, Interface and Composition Analysis on Perovskite Solar Cells, ACS Appl. Mater. Interfaces. 7 (2015) 26176−26183.
[152] D. Nanova, A.K. Kast, M. Pfannmöller, C. Müller, L. Veith, I. Wacker, M. Agari, W. Hermes, P. Erk, W. Kowalsky, R.R. Schröder, R. Lovrinčić, Unraveling the Nanoscale Morphologies of Mesoporous Perovskite Solar Cells and Their Correlation to Device Performance, Nano Lett. 14 (2014) 2735–2740.
[153] R. Ohmann, L.K. Ono, H.S. Kim, H. Lin, M.V. Lee, Y. Li, N.G. Park, Y. Qi, Real-Space Imaging of the Atomic Structure of Organic–Inorganic Perovskite, J. Am. Chem. Soc. 137 (2015) 16049–16054.
[154] J.J. Li, J.Y. Ma, Q.Q. Ge, J.S. Hu, D. Wang, L.J. Wan, Microscopic Investigation of Grain Boundaries in Organolead Halide Perovskite Solar Cells, ACS Appl. Mater. Interfaces. 7 (2015) 28518–28523.
[155] Y. Wu, A. Islam, X. Yang, C. Qin, J. Liu, K. Zhang, W. Peng, L. Han, Retarding the crystallization of PbI2 for highly reproducible planar-structured perovskite solar cells via sequential deposition, Energy Environ. Sci. 7 (2014) 2934–2938.
[156] S.M.K. Rendon, D. Mavrynsky, A. Meierjohann, A. Tiihonen, K. Miettunen, M.I. Asghar, J. Halme, L. Kronberg, R. Leino, Analysis of dye degradation products and assessment of the dye purity in dye-sensitized solar cells, Rapid Communications in Mass Spectrometry. 29 (2015) 2245–2251.
[157] L. Zhu, J. Xiao, J. Shi, J. Wang, S. Lv, Y. Xu, Y. Luo, Y. Xiao, S. Wang, Q. Meng, X. Li, D. Li, Efficient CH3NH3PbI3 perovskite solar cells with 2TPA-n-DP hole-transporting layers, Nano Research. 8 (2014) 1116–1127.

[158] L. Barnea-Nehoshtan, S. Kirmayer, E. Edri, G. Hodes, D. Cahen, Surface Photovoltage Spectroscopy Study of Organo-Lead Perovskite Solar Cells, J. Phys. Chem. Lett. (2014) 2408−2413.
[159] Y. Chen, T. Chen, L. Dai, Layer-by-Layer Growth of CH 3 NH 3 PbI 3− x Cl x for Highly Effi cient Planar Heterojunction Perovskite Solar Cells, Adv. Mater. 27 (2015) 1053–1059.
[160] H. Choi, C.K. Mai, H.B. Kim, J. Jeong, S. Song, G.C. Bazan, J.Y. Kim, A.J. Heeger, Conjugated polyelectrolyte hole transport layer for inverted-type perovskite solar cells, Nat. Commun. 6 (2014) 7348.
[161] R. Sheng, X. Wen, S. Huang, X. Hao, S. Chen, Y. Jiang, X. Deng, M.A. Green, A.W.Y. Ho-Baille, Photoluminescence characterisations of a dynamic aging process of organic–inorganic CH3NH3PbBr3 perovskite, Nanoscale. 8 (2016) 1926–1931.
[162] N. Klein-Kedem, D. Cahen, G. Hodes, Effects of Light and Electron Beam Irradiation on Halide Perovskites and Their Solar Cells, Acc. Chem. Res. 49 (2016) 347–354.
[163] C. Quarti, G. Grancini, E. Mosconi, P. Bruno, J.M. Ball, M.M. Lee, H.J. Snaith, A. Petrozza, F.D. Angelis, The Raman spectrum of the CH3NH3PbI3 hybrid perovskite: interplay of theory and experiment, J. Phys. Chem. Lett. 5 (2013) 279–284.
[164] M. Ledinský, P. Löper, B. Niesen, J. Holovský, S.J. Moon, J.-H. Yum, S.D. Wolf, A. Fejfar, C. Ballif, Raman Spectroscopy of Organic–Inorganic Halide Perovskites, J. Phys. Chem. Lett. 6 (2015) 401–406.
[165] J. Zhang, Z. Hu, L. Huang, G. Yue, J. Liu, X. Lu, Z. Hu, M. Shang, L. Han, Y. Zhu, Bifunctional alkyl chain barriers for efficient perovskite solar cells, Chem. Commun. 51 (2015) 7047--7050.
[166] H.-S. Kim, C.-R. Lee, J.-H. Im, K.-B. Lee, T. Moehl, A. Marchioro, S.-J. Moon, R. Humphry-Baker, J.-H. Yum, J.E. Moser, Lead iodide perovskite sensitized all-solid-state submicron thin film mesoscopic solar cell with efficiency exceeding 9%, Sci. Rep. 2 (2012).
[167] M.M. Lee, J. Teuscher, T. Miyasaka, T.N. Murakami, H.J. Snaith, Efficient hybrid solar cells based on meso-superstructured organometal halide perovskites, Science. 338 (2012) 643–647.
[168] C.C. Stoumpos, C.D. Malliakas, M.G. Kanatzidis, Semiconducting tin and lead iodide perovskites with organic cations: phase transitions, high mobilities, and near-infrared photoluminescent properties., Inorg Chem. 52 (2013) 9019–9038.
[169] J.-H. Im, C.-R. Lee, J.-W. Lee, S.-W. Park, N.-G. Park, 6.5% efficient perovskite quantum-dot-sensitized solar cell, Nanoscale. 3 (2011) 4088–4093.
[170] S.N. Habisreutinger, T. Leijtens, G.E. Eperon, S.D. Stranks, R.J. Nicholas, H.J. Snaith, Carbon Nanotube/Polymer Composites as a Highly Stable Hole Collection Layer in Perovskite Solar Cells, Nano Lett. 14 (2014) 5561−5568.
[171] E. Cuddihy, C. Coulbert, A. Gupta, R. Liang, Flat-Plate Solar Array Project: Final report: Volume 7, Module encapsulation, JPL Publication: Springfield, VA, USA. 7 (1986).
[172] X. Zhao, N.G. Park, Stability Issues on Perovskite Solar Cells, 2 (2015).

[173] B. Conings, J. Drijkoningen, N. Gauquelin, A. Babayigit, J. D'Haen, L. D'Olieslaeger, A. Ethirajan, J. Verbeeck, J. Manca, E. Mosconi, Intrinsic thermal instability of methylammonium lead trihalide perovskite., Adv. Energy Mater. 5 (2015) 1500477.
[174] A. Dualeh, P. Gao, S.I. Seok, M.K. Nazeeruddin, M. Grätzel, Thermal behavior of methylammonium lead-trihalide perovskite photovoltaic light harvesters., Chem. Mater. 26 (2014) 6160–6164.
[175] A. Pisoni, J. Jaćimović, O.S. Barišić, R. Gaál, L. Forró, E. Horváth, Ultra-low thermal conductivity in organic-inorganic hybrid perovskite CH3NH3PbI3., J. Phys. Chem. Lett. 5 (2014) 2488–2492.
[176] R.K. Misra, S. Aharon, B. Li, D. Mogilyansky, I. Visoly-Fisher, L. Etgar, E.A. Katz, Temperature- and component-dependent degradation of perovskite photovoltaic materials under concentrated sunlight., J. Phys. Chem. Lett. 6 (2015) 326–330.
[177] U. Bach, D. Lupo, P. Comte, J.E. Moser, F. Weissörtel, J. Salbeck, H. Spreitzer, M. Grätzel, Solid-state dye-sensitized mesoporous TiO2 solar cells with high photon-to-electron conversion efficiencies, Nature. 395 (1998) 583–585.
[178] G.E. Eperon, S.D. Stranks, C. Menelaou, M.B. Johnston, L.M. Herz, H.J. Snaith, Formamidinium lead trihalide: a broadly tunable perovskite for efficient planar heterojunction solar cells, Energy Environ. Sci. 7 (2014) 982–988.
[179] N. Pellet, P. Gao, G. Gregori, T. Yang, M.K. Nazeeruddin, J. Maier, M. Grätzel, Mixed-Organic-Cation Perovskite Photovoltaics for Enhanced Solar-Light Harvesting, Angew. Chem. Int. Ed. 53 (2014) 3151–3157.
[180] D.M. Trots, S.V. Myagkota, High-temperature structural evolution of caesium and rubidium triiodoplumbates, Journal of Physics and Chemistry of Solids. 69 (2008) 2520–2526.
[181] D.E. Scaife, P.F. Weller, W.G. Fisher, Crystal preparation and properties of cesium tin(II) trihalides, Journal of Solid State Chemistry. 9 (1974) 308–314.
[182] T. Malinauskas, D. Tomkute-Luksiene, R. Sens, M. Daskeviciene, R. Send, H. Wonneberger, V. Jankauskas, I. Bruder, V. Getautis, Enhancing thermal stability and lifetime of solid-state dye-sensitized solar cells via molecular engineering of the hole-transporting material spiro-OMeTAD., ACS Appl. Mater. Interfaces. 7 (2015) 11107–11116.
[183] Q. Luo, Y. Zhang, C.Y. Liu, J.B. Li, N. Wang, H. Lin, Iodide-reduced graphene oxide with dopant-free spiro-OMeTAD for ambient stable and high-efficiency perovskite solar cells., J. Mater. Chem. A. 3 (2015) 15996–16004.
[184] J.S. Yeo, R. Kang, S. Lee, Y.J. Jeon, N. Myoung, C.L. Lee, D.Y. Kim, J.M. Yun, Y.H. Seo, S.S. Kim, Highly efficient and stable planar perovskite solar cells with reduced graphene oxide nanosheets as electrode interlayer., Nano Energy. 12 (2015) 96–104.
[185] M.S.A. Abdou, F.P. Orfino, Y. Son, S. Holdcroft, Interaction of Oxygen with Conjugated Polymers: Charge Transfer Complex Formation with Poly(3-alkylthiophenes), J. Am. Chem. Soc. 119 (1997) 4518–4524.
[186] H. Kautsky, Quenching of luminescence by oxygen, Trans. Faraday Soc. 35 (1939) 216–219.

[187] F.T. O'Mahony, Y.H. Lee, C. Jellett, S. Dmitrov, D.T. Bryant, J.R. Durrant, B.C. O'Regan, M. Graetzel, M.K. Nazeeruddin, S.A. Haque, Improved environmental stability of organic lead trihalide perovskite-based photoactive-layers in the presence of mesoporous TiO 2, J. Mater. Chem. A. 3 (2015) 7219–7223.
[188] B. Suarez, V. Gonzalez-Pedro, T.S. Ripolles, R.S. Sanchez, L. Otero, I. Mora-Sero, Recombination study of combined halides (Cl, Br, I) perovskite solar cells, J. Phys. Chem. Lett. 5 (2014) 1628–1635.
[189] J.A. Christians, P.A.M. Herrera, P.V. Kamat, Transformation of the Excited State and Photovoltaic Efficiency of CH3NH3PbI3 Perovskite upon Controlled Exposure to Humidified Air, J. Am. Chem. Soc. 137 (2015) 1530–1538.
[190] J. Yang, B.D. Siempelkamp, D. Liu, T.L. Kelly, Investigation of CH3NH3PbI3 Degradation Rates and Mechanisms in Controlled Humidity Environments Using in Situ Techniques, ACS Nano. 9 (2015) 1955–1963.
[191] A.M.A. Leguy, Y. Hu, M. Campoy-Quiles, M.I. Alonso, O.J. Weber, P. Azarhoosh, M.V. Schilfgaarde, M.T. Weller, T. Bein, J. Nelson, P. Docampo, P.R.F. Barnes, Reversible Hydration of CH3NH3PbI3 in Films, Single Crystals, and Solar Cells, Chem. Mater. 27 (2015) 3397–3407.
[192] T. Leijtens, G.E. Eperon, S. Pathak, A. Abate, M.M. Lee, H.J. Snaith, Overcoming ultraviolet light instability of sensitized TiO2 with meso-superstructured organometal tri-halide perovskite solar cells, Nat. Commun. 4 (2013).
[193] K. Wojciechowski, T. Leijtens, S. Siprova, C. Schlueter, M.T. Hörantner, J.T. Wang, C.Z. Li, A.K.Y. Jen, T.L. Lee, H.J. Snaith, C60 as an Efficient n-Type Compact Layer in Perovskite Solar Cells, J. Phys. Chem. Lett. 6 (2015) 2399–2405.
[194] S. Schuller, Schilinsky, J. Hauch, C.J. Brabec, Determination of the degradation constant of bulk heterojunction solar cells by accelerated lifetime measurements, Appl. Phys. A. 79 (2004) 37–40.
[195] M. Jørgensen, K. Norrman, S.A. Gevorgyan, T. Tromholt, B. Andreasen, F.C. Krebs, Stability of Polymer Solar Cells, Adv. Mater. 24 (n.d.) 580–612.
[196] J. Lewis, Material challenge for flexible organic devices, Materials Today. 9 (2006) 38–45.
[197] F. Matteocci, S. Razza, F. Di Giacomo, S. Casaluci, G. Mincuzzi, T.M. Brown, A. D'Epifanio, S. Licoccia, A. Di Carlo, Solid-state solar modules based on mesoscopic organometal halide perovskite: a route towards the up-scaling process, Phys. Chem. Chem. Phys. 16 (2014) 3918–3923.
[198] H. Needleman, Lead poisoning., Annu Rev Med. 55 (2004) 209–222.
[199] Y. Finkelstein, M.E. Markowitz, Rosen, Low-level lead-induced neurotoxicity in children: an update on central nervous system effects, Brain Res. Rev. 27 (1998) 168–176.
[200] C.D. Toscano, T.R. Guilarte, Lead neurotoxicity: From exposure to molecular effects, Brain Res. Rev. 49 (2005).
[201] M. Jaishankar, T. Tseten, N. Anbalagan, B.B. Mathew, K.N. Beeregowda, Toxicity, mechanism and health effects of some heavy metals, 7 (2014) 60–72.
[202] B. Hailegnaw, S. Kirmayer, E. Edri, G. Hodes, D. Cahen, Rain on Methylammonium Lead Iodide Based Perovskites: Possible Environmental Effects of Perovskite Solar Cells, 6 (2015) 1543–1547.

[203] P. Kursula, Majava, A structural insight into lead neurotoxicity and calmodulin activation by heavy metals, Acta Crystallogr., Sect. F: Struct. Biol. Cryst. Commun. 63 (2007) 653–656.
[204] I.R. Benmessaoud, A.L. Mahul-Mellier, E. Horváth, B. Maco, M. Spina, H.A. Lashuel, L. Forró, Health hazards of methylammonium lead iodide based perovskites: cytotoxicity studies, Toxicol. Res. 5 (2016) 407–419.
[205] F.R. Stoddard, A.D. Brooks, B.A. Eskin, G.J. Johannes, Iodine Alters Gene Expression in the MCF7 Breast Cancer Cell Line: Evidence for an Anti-Estrogen Effect of Iodine, Int. J. Med. Sci. 5 (2008) 189– 196.
[206] T.T. Sherer, K.D. Thrall, R.J. Bull, Comparison of toxicity induced by iodine and iodide in male and female rats, J. Toxicol. Environ. Health. 32 (1991) 89–101.
[207] S.C. Mitchell, A.Q. Zhang, Methylamine in human urine, Clin. Chim. Acta. 312 (2001) 107–114.
[208] M. Mayer, G. Schaaf, I. Mouro, C. Lopez, Y. Colin, P. Neumann, J.P. Cartron, U. Ludewig, Different transport mechanisms in plant and human AMT/Rh-type ammonium transporters, J. Gen. Physiol. 127 (2006) 133–144.
[209] I. Guest, D.R. Varma, Developmental toxicity of methylamines in mice, J. Toxicol. Environ. Health. 32 (1991) 319– 330.
[210] J.W. Card, D.C. Zeldin, J.C. Bonner, E.R. Nestmann, Pulmonary applications and toxicity of engineered nanoparticles, Am. J. Physiol.: Lung Cell. Mol. Physiol. 295 (2008) L400–L411.
[211] M.R. Krigman, Neuropathology of heavy metal intoxication, Environ. Health Perspect. 26 (1978) 117–120.
[212] B.S. Gillis, Z. Gillis, I.M. Gavin, Analysis of lead toxicity in human cells, BMC Genomics. 13 (2012) 344.
[213] M.D. Adelaide Ross Smith, ABSORPTION OF LEAD THROUGH SKIN, 99 (1932) 2050.
[214] S.G. Lilley, T.M. Florence, J.L. Stauber, The use of sweat to monitor lead absorption through the skin., Sci Total Environ. 76 (1988) 267–278.